

BET

**Barrier Integrity of the
Isolating Rock Zone in
Clay Formations**

Final Report



Gesellschaft für Anlagen-
und Reaktorsicherheit
(GRS) mbH

BET

**Barrier Integrity of the
Isolating Rock Zone in
Clay Formations**

Final Report

Rüdiger Miehe
Oliver Czaikowski
Klaus Wieczorek

August 2010

Acknowledgement:

This report was prepared under contract No. 02 E 10116 by the Federal Ministry of Economics and Technology (BMWi).

The work was conducted by the Gesellschaft für Anlagen- und Reaktorsicherheit (GRS) mbH.

The authors are responsible for the content of the report.

GRS - 261
ISBN 978-3-939355-36-6

Keywords:

Mont Terri Rock Laboratory, Opalinus clay, Gas transport, Damage, Healing, Numerical modelling

Preface

In a high-level radioactive waste repository in a clay host rock formation which is under discussion in several European and non-European countries, gases will be produced, mainly as a consequence of corrosion of the metallic waste containers. Enough water will be available for corrosion of all metals present.

Corrosion is a slow process and will continue when engineered barriers and excavation damaged zones are fully re-saturated. Gas production may then result in a gas pressure increase, since gas flow paths in unsaturated parts of the repository are no longer available. Could the pressure exceed the minimum stress in the host rock formation, this might lead to impairment of the geological barrier by fracturing.

Therefore, the mechanism of gas transport in the saturated host rock is important for predicting the long-term behaviour of the repository.

The gas transport issue at elevated gas pressure was the subject of the BET project performed by GRS between 2006 and 2010. A combined approach involving in-situ experiments, laboratory testing, and numerical simulation was chosen.

The in-situ experiments were performed at the Mont Terri Rock Laboratory (MTRL). GRS is partner of a consortium running this underground laboratory.

For lab testing GRS runs a rock mechanics laboratory at Braunschweig.

Numerical modelling was performed using the finite element programme CODE_BRIGHT developed by the Technical University of Catalonia (UPC) in Barcelona.

This report presents the results of the BET project. The same report is published in parallel as Mont Terri Technical Note TN 2010-82.

Table of contents

1	Introduction.....	1
2	Objectives and scope of work	3
3	Mont Terri Rock Laboratory	5
4	Experimental investigations	9
4.1	In-situ testing	9
4.1.1	Test boreholes and instrumentation	9
4.1.2	Test procedure	15
4.1.3	Testing sequence	17
4.2	Laboratory testing	18
4.2.1	Core sampling and preparation.....	18
4.2.2	Experimental procedure.....	20
4.2.3	Fracture visualisation	23
5	Experimental results	25
5.1	In-situ measurements	25
5.1.1	Pore pressure	25
5.1.2	Water injection tests February and August 2007.....	26
5.1.3	Gas injection tests November 2007	27
5.1.4	Gas injection tests May 2008.....	29
5.1.5	Water injection tests May/June 2008	30
5.1.6	Water injection tests September 2009	31
5.1.7	Gas injection tests December 2009	31
5.2	Laboratory testing	37
5.2.1	Small samples	37
5.2.2	Large samples	43
5.2.3	Fracture images.....	48

6	Numerical investigations	51
6.1	Physical modelling	51
6.1.1	Theoretical framework	51
6.1.2	Balance equations	52
6.1.3	Equilibrium restrictions.....	53
6.1.4	Constitutive equations	54
6.1.5	Material parameters.....	56
6.2	Numerical simulation	57
6.2.1	Model geometry and boundary conditions	57
6.2.2	Calculation sequence	59
6.3	Analysis and interpretation.....	60
7	Discussion	69
7.1	In-situ investigations	69
7.2	Laboratory results	72
7.3	Numerical investigations.....	74
7.4	Comparison to rock salt behaviour.....	77
8	Conclusions	79
	References	81
	List of figures.....	85
	List of tables	89

1 Introduction

A central issue discussed in the criteria for the selection procedure of repository sites for radioactive waste disposal in Germany, as compiled by the „Arbeitskreis Auswahlverfahren Endlagerstandorte“ (AkEnd) /AKE 02/, is the confirmation of the integrity of the isolating rock zone (IRZ). The isolating rock zone is defined as the part of the geologic barrier which, together with the geotechnical barriers, has to ensure the safe containment of the waste in such a way that it essentially remains at the site of emplacement and that not more than minimal defined quantities of material are able to leave that IRZ /BMU 09/.

The evolution of elevated gas pressure as a consequence of anaerobic corrosion of waste containers or radiolysis of water contained in the host rock cannot be excluded a priori. According to Rübél /RUE 04/, /RUE 05/ clay formations contain sufficient pore water to corrode all emplaced high-level waste canisters. 481 Nm³ (m³ at normal conditions) of hydrogen gas per canister could be produced.

Different mechanisms of gas migration in clay formations do exist:

- Dissolution of the gases in the pore water and diffusion in the liquid phase
- Diffusive and advective transport in the gas filled pore volume of the host rock if the rock is not fully saturated
- Two phase gas-water flow in the pore volume of the host rock if the gas entry pressure is exceeded and water is displaced
- Gas flow on micro-fracs if the gas pressure exceeds the minimum principal stress and micro-fracs are generated (dilatancy-controlled gas flow)
- Gas flow on macro-fracs if the gas pressure exceeds the minimum principal stress and the gas generation rate is so high that the gases cannot be drained off through the micro-fracs

If gas transport is hindered due to full water saturation of the host rock and the geotechnical barriers, a high gas pressure could evolve. In case of the gas pressure exceeding the minimum principal stress in the rock, the last two of the above mechanisms are possible. Discrete fracturing could occur which would significantly impair the integrity of the host rock. Gas propagation along a damaged bedding plane

was observed in the frame of the Mont Terri heater test HE-D /ZHA 07/, although the respective tests were performed in the formerly heated region of the HE-D, which cannot be considered as undisturbed rock.

It is, however, expected that after discharge of the gas swelling of the clay rock can lead to a re-sealing of the fractures /ZHA 02/, /ZHA 04/.

In order to assess the consequences of gas production in a repository, knowledge about the formation and possible re-sealing of transport paths in the rock and about the parameters influencing the transport processes, including the temporal evolution of these effects, is required.

The investigation of the relevant mechanism of gas transport in the isolating rock zone of a repository in claystone is subject of the BET project. The project comprises in-situ and laboratory experiments for identifying the relevant processes and quantifying the expected alterations in the hydraulic properties. Additional coupled hydraulic-mechanical modelling has been performed in order to find out in how far existing material models are able to reproduce the observed phenomena.

The investigations performed in the frame of BET concentrated on gas transport at elevated gas pressure (in the range of the minimum principal rock stress). Gas transport at lower pressure was the main topic of the project HG-C which was finished at the end of 2008 /JOC 08/. In the HG-C, the following main results were obtained:

- In the undisturbed region several metres from the opening, the rock is water saturated, and no advective flow occurs below the gas entry pressure. The relevant gas migration mechanism is diffusion of dissolved gas in the liquid phase. For different tracer gases, effective diffusion coefficients ranging between 10^{-12} m²/s and 10^{-10} m²/s were determined. There is a clear dependence on molecular mass of the tracer.
- Gas entry pressures between 2 and 3.4 MPa were found during constant pressure injection tests. When repeating an injection test, the second entry pressure is somewhat lower. In most cases, gas flow is restricted to the bedding planes. The most probable mechanism at higher pressure is dilatancy controlled gas flow. Effective permeabilities to gas in the range of 10^{-21} to 10^{-19} m² were determined.

2 Objectives and scope of work

The overall objectives of BET were to identify the relevant mechanisms of gas transport in undisturbed clay rock at pressures close to or exceeding the minimum principal stress and to improve their understanding, to measure the hydraulic properties under such conditions, and to investigate potential re-sealing after gas-pressure induced pathway generation. Specifically, the following questions were addressed:

- Is gas entry at high pressure controlled by dilatancy, i. e., by expansion of the pore system resulting in limited damage and an increase of permeability, or by the formation of discrete fractures?
- What are the gas entry pressures and the effective gas permeabilities after gas entry?
- Are gas pathways re-sealed after re-saturation, and what is the time scale for this?

The work programme designed to investigate the above questions was structured in three major sections:

- In-situ investigations: Several series of injections tests were performed in boreholes in the Mont Terri Rock Laboratory. The tests comprised water injection tests and pore water pressure measurement to characterise the rock in its initial state and gas injection tests to determine gas entry pressure and effective permeability. The tests were repeated after different time intervals allowing for self-sealing.
- Laboratory experiments: Laboratory tests aimed at inducing damage in rock samples by gas pressure at various mechanical loads and injection rates and investigating the formation and properties of pathways as well as at investigating the self-sealing behaviour under in-situ relevant stress conditions. Additional tests on large samples were performed to check the scale-effect.
- Modelling: The finite element code CODE_BRIGTH was used to perform coupled hydro-mechanical modelling to check in how far the observed phenomena could be described by a simple elastic model with two-phase flow.

3 Mont Terri Rock Laboratory

The Mont Terri Rock Laboratory (MTRL) is situated in the north-western part of Switzerland, where it has been excavated parallel to the security gallery of the Mont Terri motorway tunnel on the south-western slope of the Mont Terri anticline (fig. 3.1 and 3.2). It is located in the Opalinus clay formation consisting of three main facies: the sandy facies, the shaly facies, and the sandy carbonate-rich facies. More details about the different lithologies can be found in /THU 99/. The bedding planes plunge towards the south-east with an azimuth of $140^{\circ} - 150^{\circ}$. The apparent thickness of the Opalinus clay is about 160 m. Its current overlay varies between 250 and 320 m, while it is estimated to have reached at least 1000 m in the past. The clay rock is saturated with water, but water circulations are practically negligible due to its very low permeability and pressure gradient. In the regions far from the openings in the MTRL the pore-water pressure amounts to values around 2 MPa and the rock temperature is about 15°C .



Fig. 3.1 Mont Terri motorway tunnel and location of the Mont Terri Rock Laboratory (left centre of the picture)

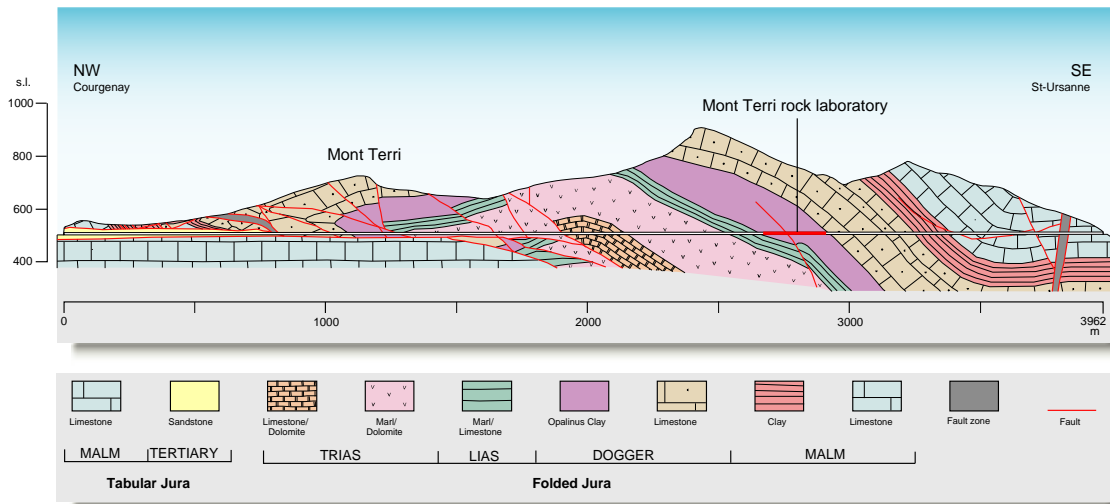


Fig. 3.2 Geological profile along the motorway tunnel showing the location of the Mont Terri Rock Laboratory

The state of stress at the MTRL is estimated according to /BOS 03/:

- the maximum principal stress σ_1 with a magnitude range of 6 – 7 MPa and a sub-vertical direction of 210° azimuth and 70° dip,
- the intermediate principal stress σ_2 with a magnitude range of 4 – 5 MPa and a sub-horizontal direction of 320° azimuth and 10° dip (sub-parallel to the motorway tunnel and the security gallery), and
- the minimum principal stress σ_3 with a magnitude range of 2 – 3 MPa and a sub-horizontal direction of 50° azimuth and 20° dip (more or less normal to the motorway tunnel and the security gallery).

The BET test site is located in the shaly facies. An overview of the rock laboratory with the locations of the BET site and of additional testing boreholes is shown in fig. 3.3. Figure 3.4 shows a plan view of the laboratory including geological information.

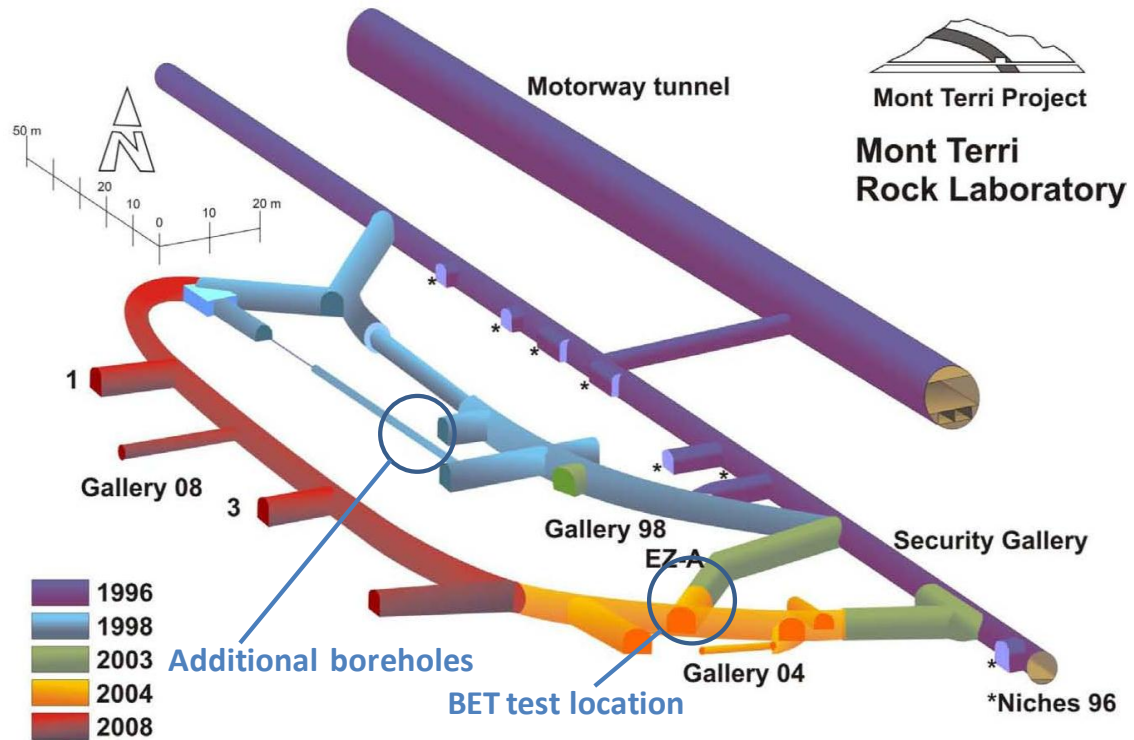


Fig. 3.3 View of the Mont Terri Rock Laboratory showing the various tunnels with the year of their excavation and the BET experimental sites

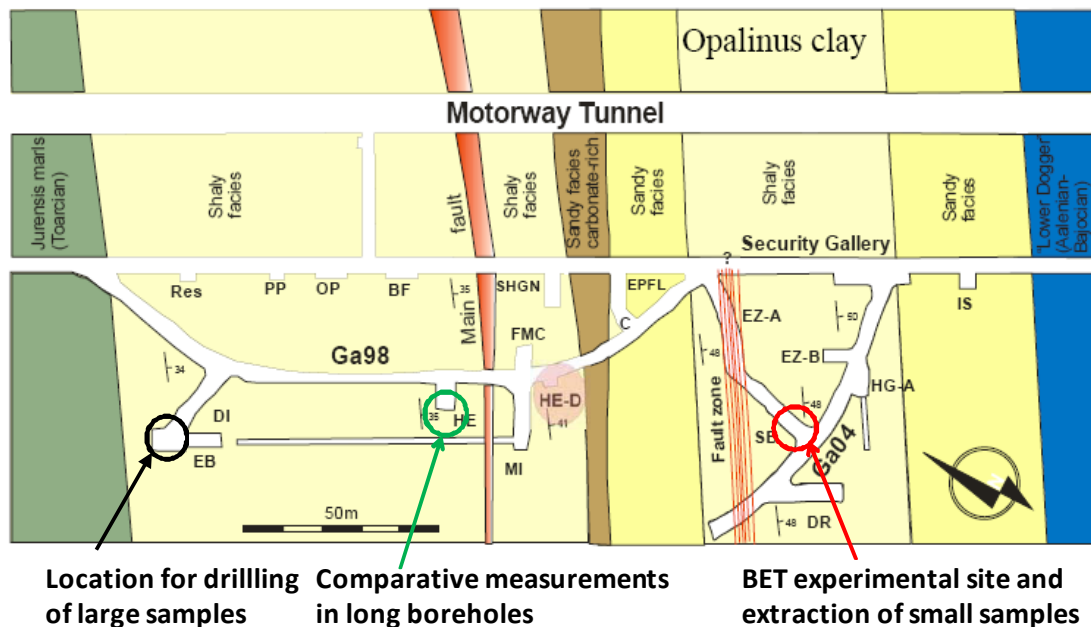


Fig. 3.4 Plan view showing the Mont Terri Rock Laboratory geology

4 Experimental investigations

The experimental investigations performed at the MTRL and the GRS laboratory at Braunschweig are described in this chapter; the results are presented in chapter 5.

4.1 In-situ testing

4.1.1 Test boreholes and instrumentation

4.1.1.1 BET test site

For the in-situ measurements six boreholes were drilled and instrumented at the BET experimental site in the MTRL (see fig. 3.3 and 3.4) in December 2006. All boreholes have a 45° downward inclination (see fig. 4.1), three of them (BET 1, BET 2, and BET 3) are oriented parallel to the bedding and the other three (BET 4, BET 5, and BET 6) perpendicular to the bedding.

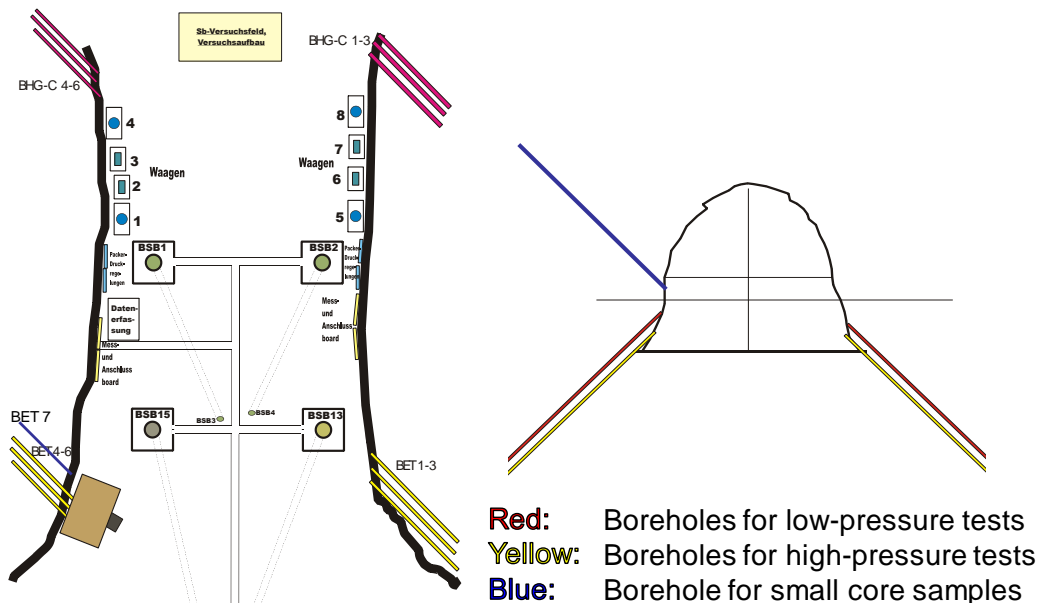


Fig. 4.1 Boreholes at the BET test site

(Boreholes used for the HG-C experiment in red, test boreholes BET 1 – BET 6 in yellow, sampling borehole BET 7 in blue. The boreholes parallel to the bedding (BET 1 – BET 3) are drilled from the right wall, the ones perpendicular (BET 4 – BET 6) from the left)

All six test boreholes have a diameter of 20 mm, but different lengths: 6 m (BET 1 and BET 4), 8 m (BET 2 and BET 5), and 10 m (BET 3 and BET 6). Figure 4.2 shows a photo of the drilling procedure.



Fig. 4.2 Drilling of test boreholes

The boreholes were instrumented with minipiezometer probes, which consist of a 40 cm long sintered steel tube (outer diameter 18 mm, inner diameter 8 mm), which is mounted on a steel capillary. A second capillary is connected to the upper end of the sintered tube, so that gas or water can be circulated through the probe (fig. 4.3).

In each of the test boreholes a probe was placed at maximum depth. Above the sintered steel tube the probe was equipped with Hilti cement which was pressed to the borehole wall after placing the probe, using the drilling rod. In order to completely seal the piezometer in the rock the remaining borehole void above each piezometer was backfilled with synthetic resin (Sikadur 52).



Fig. 4.3 Minipiezometer installed in the test boreholes

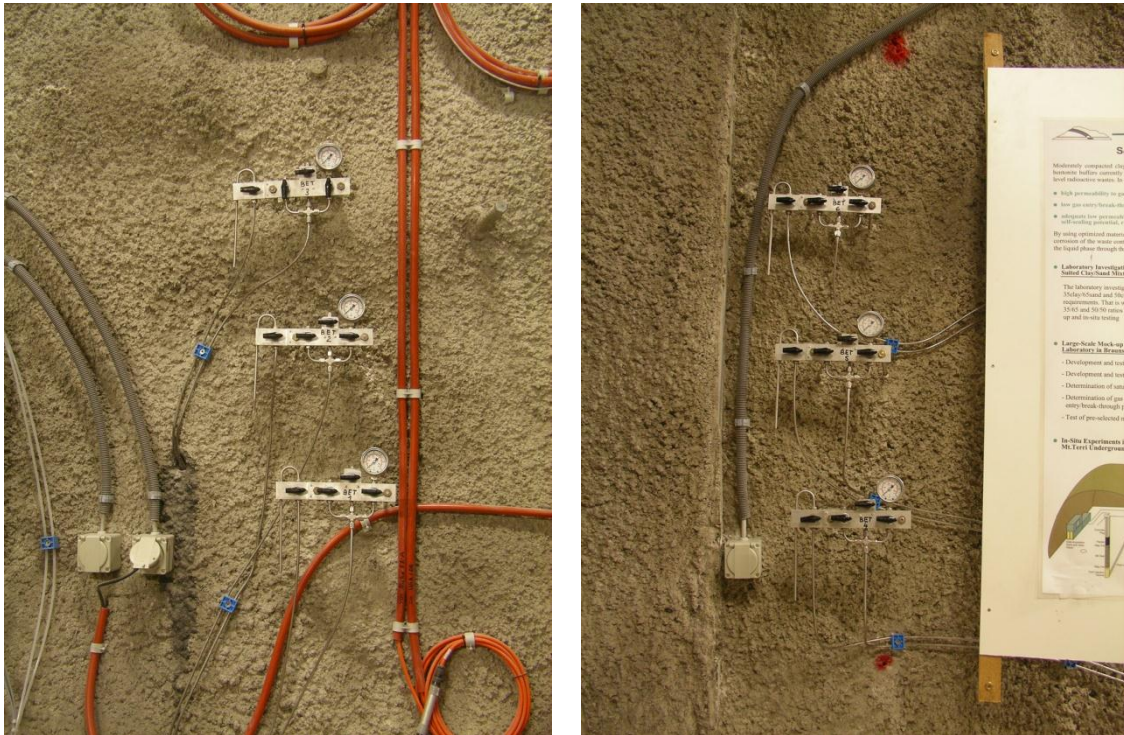


Fig. 4.4 Transducer rack: BET 1-3 (left) und BET 4-6 (right)

The steel capillaries of the piezometers were connected to transducer racks equipped with pressure gauges and pressure transducers located near the borehole collars (see fig. 4.4). After finishing the installation, the measuring intervals of the piezometer probes were filled with artificial pore water (Pearson water). The water was injected via the capillary attached to the lower end of the piezometer and the valve of the upper end capillary was opened in order to enable elusion of the air contained in the probe. After

filling the complete probe volume injection and return valves were closed. During the procedure, it was found that the return tube of BET 1 was blocked. Therefore, the air in the test interval of BET 1 could not be released.

In addition to the borehole instrumentation, two precision balances were available to measure gas or water mass during the injection tests.

The pressure and balance data in the BET project (and also in the SB and HG-C projects) were collected and processed by use of a GeoMonitor system of Solexperts AG. The principle layout of the system is shown in fig. 4.5.

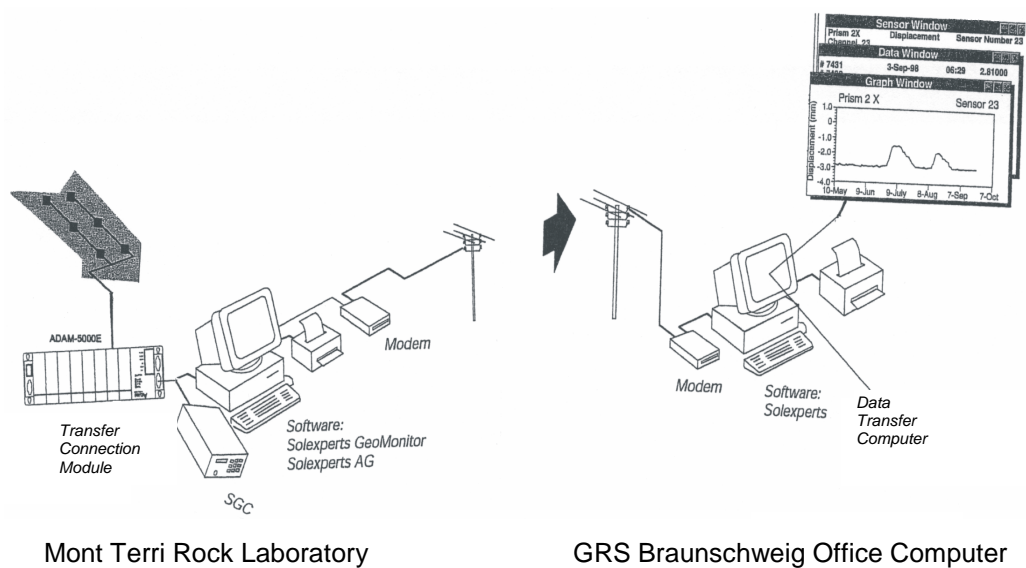


Fig. 4.5 Principle layout of the Data Acquisition System (DAS)

4.1.1.2 HE-B niche

During the measurements in the BET boreholes it was found that most probes showed no elevated pore pressure (see section 5.1.1). This gave reason to doubt that the probes were located in a hydraulically undisturbed part of the rock. A pore pressure below the atmospheric pressure is a sign for suction, which, in a clay rock, means the rock is not fully saturated. In order to make sure that relevant results were produced by the measurements, additional tests were performed in two long boreholes drilled from the HE-B Niche (see fig. 4.6).

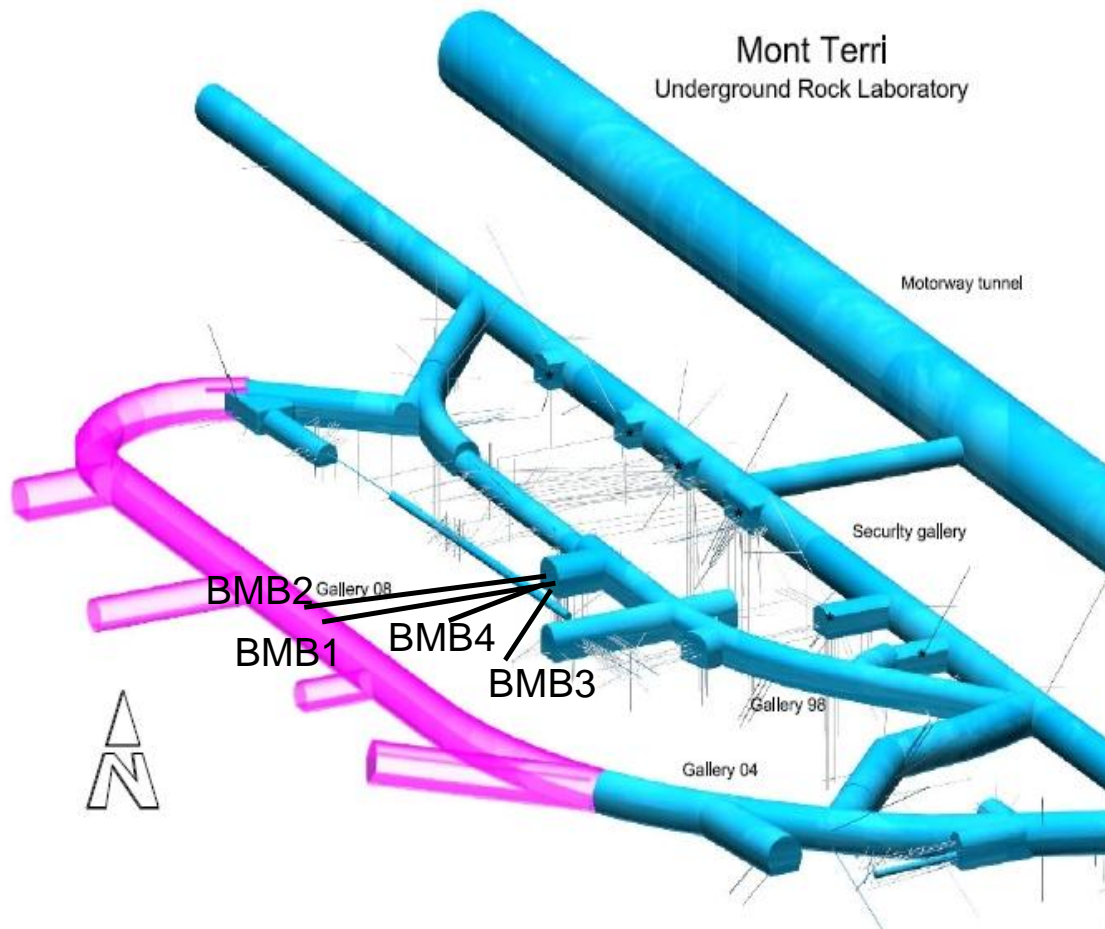


Fig. 4.6 Boreholes BMB 1 – BMB 4 drilled from the HE-B Niche

The four 42-mm boreholes BMB 1 – BMB 4 were drilled in October 2007 in the frame of the preparatory work for a mine-by experiment performed at the MTRL. Two 37 m and 38 m long boreholes (BMB 1 and BMB 2) were drilled subhorizontally into the region of the planned Gallery 08 in order to measure pore pressure changes during the gallery excavation. Two additionally boreholes (BMB 3 and BMB 4) with a length of 24 m each were drilled 45° inclined downward into the region below the centre of the pillar below the existing Gallery 98 and the future Gallery 08 (see fig. 4.6). These two boreholes were used in the frame of BET for additional measurements, since they are located positively in an undisturbed region of the rock.

Instead of a sintered steel probe, the BMB boreholes were instrumented with sliding-end minipacker probes as shown in fig. 4.7. The borehole voids above the minipackers were again backfilled with synthetic resin.



Fig. 4.7 Boreholes BMB 1 – BMB 4 drilled from the HE-B Niche

The injection and return tubes (steel capillaries) were again connected to transducer racks (fig. 4.8) and the test intervals of the boreholes filled with Pearson water. The transducers were connected to a small stand-alone GeoMonitor system which is similar to the one used for the other boreholes.



Fig. 4.8 Borehole collars of BMB 1 – BMB 4 and transducer racks (left)

4.1.2 Test procedure

4.1.2.1 Pore pressure

During the times before and in between the injection tests, the pressure recorded in the probes can be interpreted as pore pressure of the adjacent rock.

4.1.2.2 Permeability to water

Water injection tests were performed in the boreholes to characterise the state of the rock adjacent to the probes in terms of permeability. Pearson water was injected by a manual pump causing a increased pressure of 0.5 MPa to 1.9 MPa in the respective interval, depending on the original pore pressure. The injected amount of water was measured using a precision balance. After injection, the valves were closed and the pressure decay by flow into the rock was recorded.

For evaluating the pressure decay curves in terms of permeability, the code WELTEST 200 was used. WELTEST 200 provides means to calculate the analytic solution to the diffusion equation or to numerically model pressure distribution in one- or two-dimensional models, and to iteratively minimize the deviation between the measured and calculated pressure data.

The parameters affecting the calculated pressure evolution are the rock permeability, the rock porosity, the wellbore storage coefficient, and the skin factor. The skin factor accounts for an increased or decreased permeability of a zone close to the borehole wall, which can be due to the drilling procedure. For the BET tests, no skin factor was regarded.

The calculated pressure curves are rather insensitive to changes in porosity. The porosity was held constant at 15 %; changing the porosity by a factor of ten has no significant influence on the best fit permeability. Wellbore storage is important during the injection phase and controls the peak pressure reached during injection. The pressure curve form, especially during the shut-in phase, is controlled by the permeability. The best-fit permeability was determined by two-dimensional isotropic calculation, hydraulic anisotropy was not considered for the evaluation.

4.1.2.3 Gas entry pressure

Prior to measuring gas entry pressure, the respective test interval was purged with nitrogen and the water was displaced. Gas entry pressure was then determined by injecting nitrogen into the test interval at different pressure steps and measuring the resulting gas flow. In order to do this, the nitrogen tank was placed on the precision balance and the weight loss of the tank was measured. After the first detection of a gas flow, the pressure was increased further until a stable flow was achieved. Subsequently, gas pressure was reduced until the gas flow ceased.

4.1.2.4 Effective permeability to gas

The pressure steps at which a stable gas flow was achieved during the gas injection tests were evaluated in terms of effective permeability to gas, using the radial formulation of the Darcy equation for compressible fluids (eq. 4.1, see section 4.2.2).

It is understood that this kind of evaluation does not really yield a permeability value for the rock. The Opalinus clay is highly water saturated, and the conditions for a laminar flow in a porous medium do not hold for the gas injection tests. In particular, as will be shown in chapter 5, the pore space available for the gas flow is not constant, but is opened with the flow and reduces again when the pressure is reduced. Therefore, the preconditions for Darcy flow are not given. This kind of evaluation still makes some sense, because it yields a „permeability“ value which is useful for characterising the observed gas flow, even if it does not strictly comply with the physics of the flow. This permeability will in the following considerations be called „apparent permeability“.

4.1.2.5 Detection of self-sealing

Potential self-sealing of the rock adjacent to the piezometers was investigated by repetitive water and gas injection testing after varying disturbance-free time intervals. The idea was that repeating a gas injection test after having induced some damage in the rock will lead to a lower gas entry pressure, ideally the shut-in pressure at which gas flow ceases. If self-sealing takes place, the original gas entry pressure will be restored.

Two different time intervals and strategies were used:

- Gas was left in the test intervals after gas injection testing, and the gas injection tests were repeated after 6 months.
- After gas injection testing, the gas was replaced by Pearson water and new gas injection tests were performed 18 months later.

4.1.3 Testing sequence

The complete sequence of in-situ testing is compiled in the following tab. 4.1. Different colours are used for distinguishing between water and gas injection phases.

Tab. 4.1 Sequence of in-situ testing

Date	Activity	Comment
December 2006	Drilling and installation of BET 1 - BET 6	Test site preparation
February 2007	First water injection tests BET 1 - BET 6	Characterisation of initial state
August 2007	Second water injection tests BET 1 - BET 6	
November 2007	First gas injection tests BET 2 and BET 5	Determination of gas entry pressure
May 2008	Gas injection tests BET 1 - 2 and BET 4 - 6	
May/June 2008	Water injection BET 1 - BET 6	Start of Self-sealing phase
September 2009	Water injection tests BET 1 – BET 6 and BMB 3 / BMB 4	(Comparison to) initial state
December 2009	Gas injection tests BET 1 - BET 6 and BMB 3 / BMB 4	Determination of gas entry pressure

4.2 Laboratory testing

The procedures of core sampling and preparation, the laboratory testing methods and the means of fracture visualisation are described in this section.

4.2.1 Core sampling and preparation

4.2.1.1 Small samples

A borehole for obtaining core samples from the BET test site was drilled in January 2007 (BET 7, see fig. 4.1). The borehole had a total length of 7.9 m and provided cores of 100 mm diameter parallel to the bedding. Close to the tunnel wall, no intact samples which could be used for lab testing were obtained. At distances of more than about 3 m from the tunnel wall, suitable cores were obtained.

In order to reduce changes in the cores induced by de-saturation or unloading as far as possible, the samples were prepared on-site, directly after extraction.

Right after drilling, the cores were cut to a length of about 20 cm. Samples used for radial flow tests received an axial drill hole of 4 mm diameter.

The samples were shrink-wrapped in two layers of aluminium-coated foil and placed in slitted PVC tubes. Between the foil layers a wet cloth was placed to avoid drying of the sample. The end faces were equipped with rubber discs and PVC plates which were loaded with a strap to avoid axial unloading. Then, the PVC tubes were loaded with metal clamps in order to avoid radial unloading. The complete assembly was afterwards sealed with silicon mass to provide protection from de-saturation. Figure 4.9 shows the individual steps of sample conditioning.



Sample after drilling.



Sample supplied with aluminium coated plastic wrap and slitted PVC tube.



Sample installed in the PVC tube with rubber discs (front) and PVC stoppers (back) for the end planes.



Sample installed in PVC tube with clamping device for axial clamping.



Axially clamped sample.



Radially clamped sample using clamping collar.

Fig. 4.9 Preparation of the small core samples

4.2.1.2 Large samples

After unsuccessful attempts to core large samples from the BET test site, three large cores with a diameter of 255 mm could be obtained from a vertical down borehole in the northwest part of the MTRL (see fig. 3.4). With regard to the sample axis, the bedding is inclined by about 45°. The samples were shrink-wrapped in aluminium-

coated foil and placed in a pair of half-shells. Radial unloading was prevented using straps, axial load was imposed by a rod fixture.

When the first sample was removed from the fixture a failure along a bedding plane occurred, so that the sample could not be used. The second sample showed weakness along a bedding plane, but remained intact. Therefore, this sample was reconstructed by cementing two steel rods in drill holes parallel to the sample axis. The sample was used for testing because it was not yet clear whether the third sample would be intact. Moreover, this sample provided the occasion to investigate a damaged rock with the nature of the damage being known beforehand, with a fracture that was expected to be comparable to an in-situ frac. This sample had a diameter of 255 mm and a length of 390 mm.

The third sample, with the same diameter and a length of 510 mm remained intact. The preparation of this sample and the installation in the MTS testing apparatus at the GRS laboratory is shown in fig. 4.10.

In order to be able to establish a radial flow in the samples, an axial central borehole of 32 mm diameter was drilled which could serve as injection borehole for water or gas. For mechanical support a punched plate was placed on the outer surface and soldered. For collecting the measuring fluid injected in the central borehole on the perimeter, a thin sand layer was put between the punched plate and the rubber jacket in which the sample was embedded. The measuring fluid was led from the sand layer to flowmeters outside the apparatus.

4.2.2 Experimental procedure

The following tests on small samples (100 mm diameter, 200 mm length) were performed:

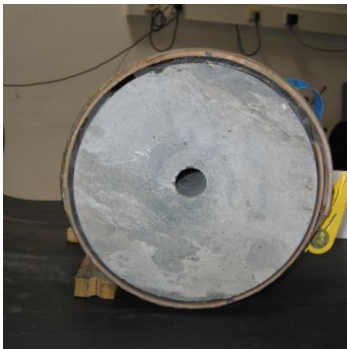
- Gas injection tests to investigate the dependence of gas permeability on the injection pressure under isostatic load at ambient temperature
- Gas injection tests under isostatic load at elevated temperature
- Gas injection tests to investigate the dependence of gas permeability on the injection pressure under triaxial load conditions



Intact large Opalinus clay sample.



Covering the sample with a punched plate, soldering the seam of the plate.



Central borehole.



Clamped sample after preparation.



Installing the sample in the MTS test apparatus. Support straps were removed before complete installation.



Sample embedded in rubber jacket in the MTS test apparatus.

Fig. 4.10 Preparation of a large core sample

For the large samples (damaged and intact), the following test succession was used:

- Gas injection tests to investigate the dependence of gas permeability on the injection pressure under triaxial load conditions
- Water injection to re-saturate the sample

- Stepwise gas injection for determining gas entry pressure
- Measurement of effective gas permeability after gas entry

For investigating the hydraulic behaviour of the samples the measuring fluid (water or gas) was injected into the central drill hole and flowed radially to the sand-filled annulus at the outer perimeter. The samples were isolated at the ends, so that axial flow was suppressed.

For gas injection moisturised nitrogen was used to avoid drying of the sample. Injection pressure was increased stepwise, starting with low pressure. Additional tests at increased temperature (maximum 90 °C) were performed using the small samples.

For investigation of the self-sealing behaviour, water injection tests with Pearson water were performed on the large samples in succession to the gas tests.

Gas flow rates in the samples were determined by measuring the displacement of a water column in a burette. Water flow rates were measured by continuously weighing the water leaving the sample.

The permeability of a sample to gas in the case of radial flow is calculated by the respective Darcy formulation for compressible media:

$$k_{grad} = \frac{q_g \cdot \mu_g \cdot p_e \cdot \ln \frac{r_e}{r_w}}{\pi \cdot h \cdot (p_w^2 - p_e^2)} \quad (4.1)$$

For incompressible liquids the following equation is used:

$$k_{wrad} = \frac{q_w \cdot \mu_w \cdot \ln \frac{r_e}{r_w}}{2\pi \cdot h \cdot (p_w - p_e)} \quad (4.2)$$

With (see fig. 4.11)

k_{grad}	gas permeability for radial flow, m ²
k_{wrad}	water permeability for radial flow, m ²
p_e	pressure in the annulus (in these tests atmospheric pressure), Pa
p_w	pressure in the central injection drillhole, Pa
r_e	radius of the sample, m

r_w	radius of the central drill hole, m
h	height of the sample, m
μ_g	viscosity of the gas, Pa·s
μ_w	viscosity of the water, Pa·s

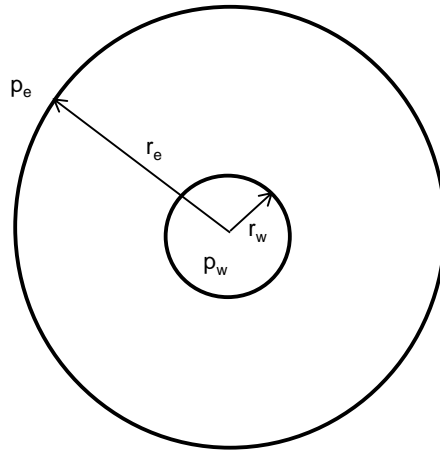


Fig. 4.11 Symbolic sample cross section with denotation of variables for permeability calculation

4.2.3 Fracture visualisation

In order to get a visual impression of the fractures existing in the core samples it was originally planned to inject a synthetic resin augmented with uranine tracer. A sample of 199.9 mm length and 100.7 mm diameter was meant to be cut in thin slices and the resin that penetrated the fractures visualised in ultraviolet light. This, however, was not successful. Therefore, a sample was machined down from the end face by 2 mm layers and each uncovered layer was scanned with a resolution of 1600 dpi. From a starting position the sample was turned by 40°, 50°, and 60°. Using the image analysis code IMAGEJ /ABR 04/, RAS 09/ for two-dimensional representations the fractures in each layer were digitised, so that they were available in plane coordinates. By combination of the datasets of all the layers a three-dimensional representation of the fractures was obtained.

5 Experimental results

5.1 In-situ measurements

The in-situ measurement results obtained from early 2007 to end of 2009 are presented in this section.

5.1.1 Pore pressure

The pressure evolution in the test intervals of the BET boreholes until start of the first gas injection tests in November 2007 is shown in fig. 5.1. With the exception of BET 6, all transducers showed pressures comparable to the atmospheric pressure or below. The first idea that this could be caused by the disturbance introduced by drilling was dropped when after the water injection tests in February and in August 2007 the pressure always returned to these low values.

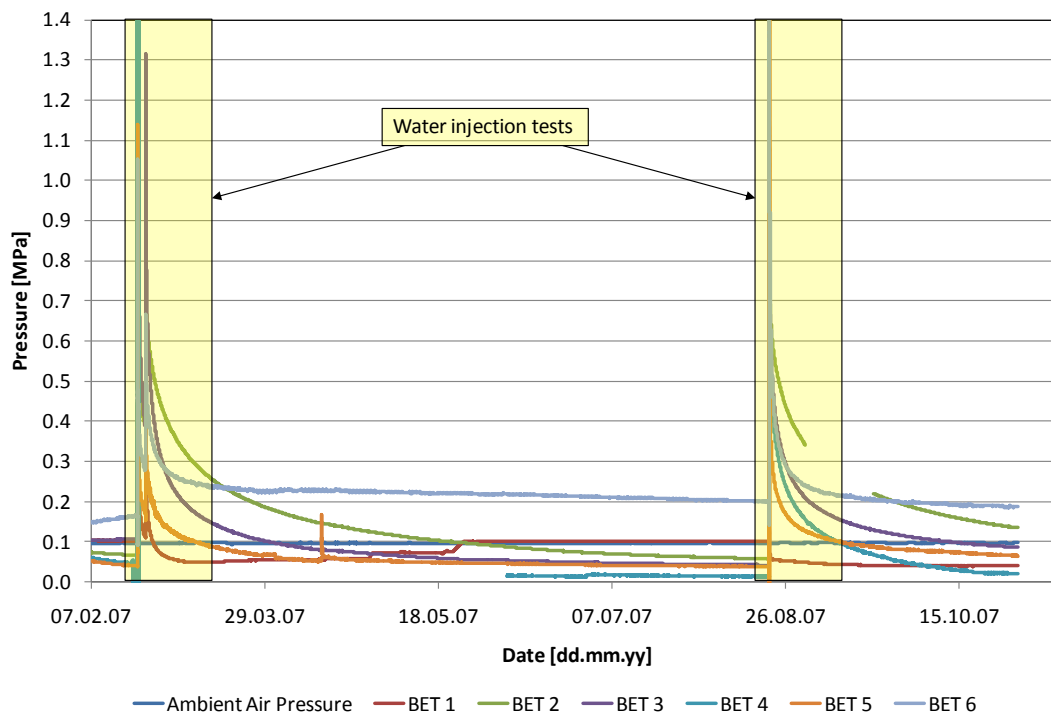


Fig. 5.1 Pressure evolution in the BET boreholes before the first gas injection tests

The advanced numerical simulations performed in the meantime (see section 6.3) explain the observed pressures as a result of the gallery excavation and ventilation. They also show that the rock is most likely fully saturated in a technical sense.

After the first gas injection tests the pressure is permanently disturbed in the vicinity of the test intervals, and an interpretation of the pressure readings as rock pore pressure is no longer possible.

In the BMB boreholes an elevated pore pressure was recorded throughout the monitoring time. After installation in October 2007 and a subsequent equilibration time of about three months pore pressure remained between 0.5 MPa and 1.1 MPa until the water injection tests were performed in September 2009 (fig. 5.2). The reasons for the pressure drops at BMB 3 in May 2009 and at BMB 4 after the water injection in September 2009 are, however, unclear.

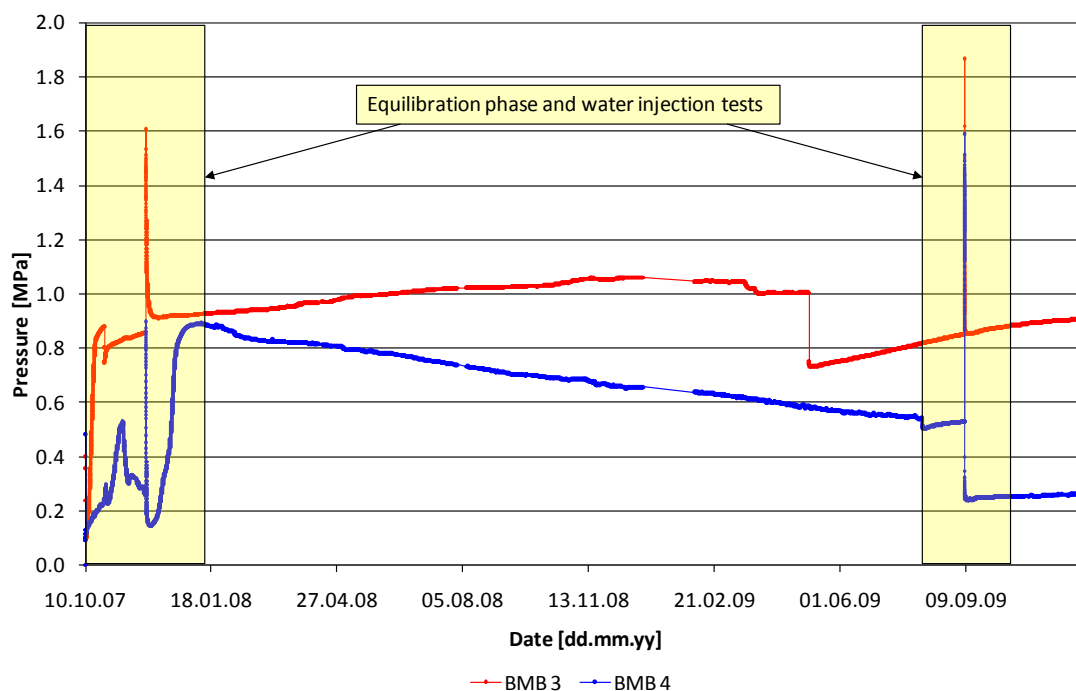


Fig. 5.2 Pressure evolution in the BMB boreholes before the gas injection tests

5.1.2 Water injection tests February and August 2007

In February and in August 2007 water injection tests were performed in order to determine the permeability to water of the rock close to the test intervals (see fig. 5.1). The pressure curves were evaluated with WELTEST as described in section 4.1.2.2.

The permeability values obtained were rather homogeneous, except for BET 1 and BET 6 all permeabilities were in the range of 10^{-19} m^2 . The permeability at BET 6 ranged at $2 \cdot 10^{-20} \text{ m}^2$. The tests at BET 1 resulted in a value of $2 \cdot 10^{-16} \text{ m}^2$, which is, however, not reliable since due to the blocked return tube the gas in the test interval could not be removed.

The complete data are given in tab. 5.1 in section 5.1.5 together with the results of the later water injection tests.

5.1.3 Gas injection tests November 2007

On November 28 and 29, 2007 the first gas injection tests were performed in test intervals BET 2 and BET 5. On November 28, the two intervals were stepwise loaded with gas pressure until a gas flow was observed. The procedure was repeated on November 29. The measured data for BET 2 are shown in fig. 5.3.

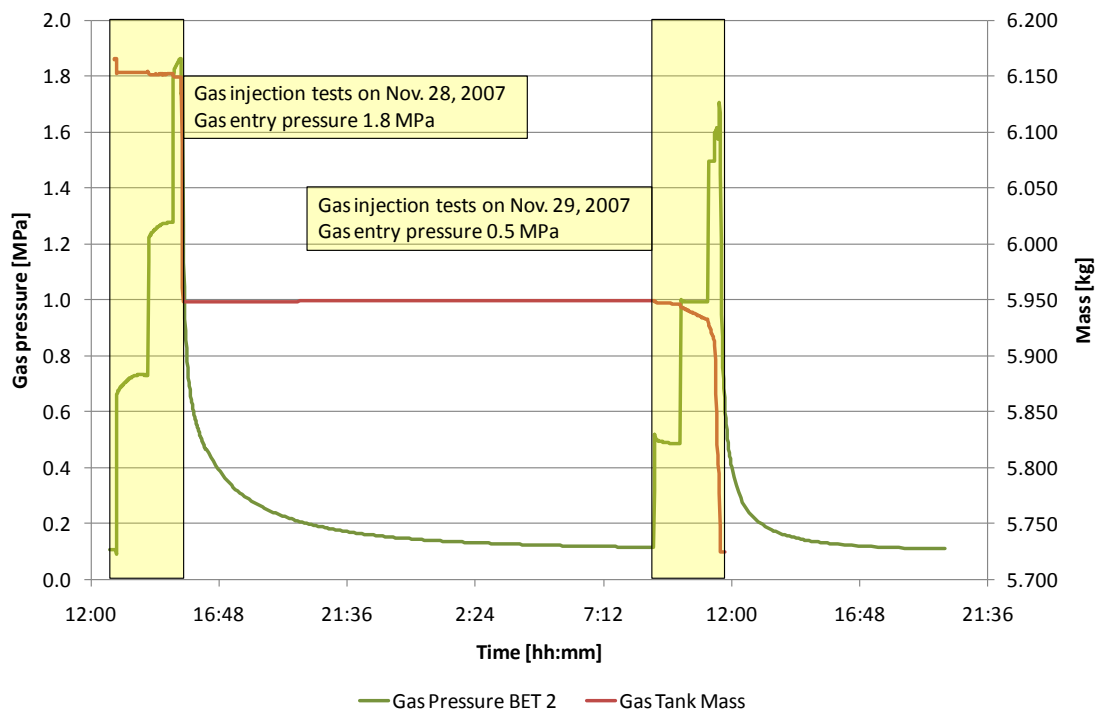


Fig. 5.3 Gas injection BET 2 in November 2007: Gas injection pressure and gas tank mass

On the first injection day, a gas entry was observed at a pressure of 1.8 MPa at BET 2. After a short flow phase during which 200 g of nitrogen flowed into the rock the valve was closed and the pressure in the interval decayed. On the following day, a gas flow

into the rock was already detected 0.5 MPa injected pressure. The pressure was raised in several steps, and with each step the flow rate increased. The flow rate at each step was nearly constant, so that data obtained during the individual pressure steps could be used to determine apparent steady-state gas permeabilities. The resulting values were in the range from 10^{-18} m^2 to 10^{-16} m^2 and showed a clear dependence on injection pressure. The complete apparent gas permeability data are compiled in tab. 5.3 in section 5.1.7, the gas entry pressures are compiled in the tab. 5.2 in the same section.

At BET 5, increasing the gas injection pressure in several steps to 2.4 MPa did not seem to result in a gas flow. But some time after shutting of the gas tank pressure started to decrease, meaning that gas flowed into the rock. A similar behaviour had already been found during gas injection tests performed in the frame of the HG-C project /JOC 08/. This observation supports the view that dilatant opening of pathways which is a more or less continuous process is relevant with respect to gas transport in the clay rock. The behaviour seen here is definitely not connected to a gas-frac.

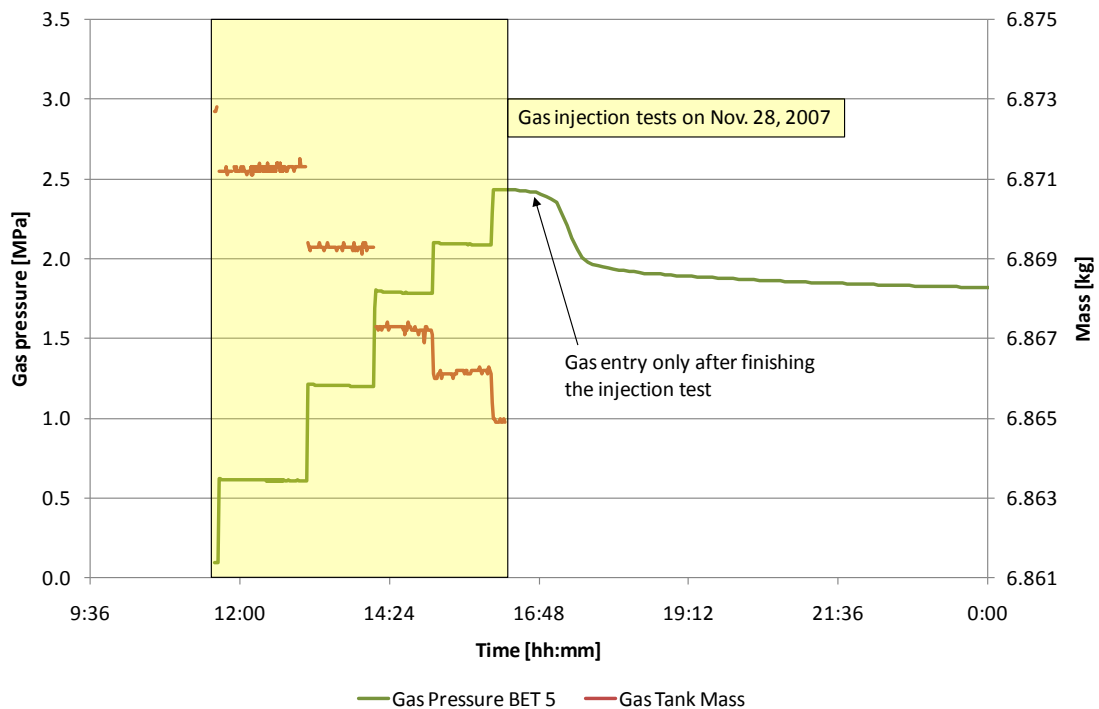


Fig. 5.4 Gas injection BET 5 in November 28, 2007: Gas injection pressure and gas tank mass

On the following day gas injection was repeated with several pressure steps. Again, the apparent gas permeability rose significantly with the injection pressure (see tab. 5.2 and tab. 5.3 in section 5.1.7 for the complete data).

5.1.4 Gas injection tests May 2008

In May 2008 another series of gas injection tests was performed. The test intervals BET 2 and BET 5 had not been re-saturated in the meantime, instead, the gas had been left in the system.

The gas entry pressures at BET 2 and BET 5 were considerably lower than during the first measurements; for BET 2 it was between 0.6 MPa and 1.2 MPa and for BET 5 between 1.25 MPa and 1.85 MPa. Figure 5.5 shows the measurement curves of BET 2 as an example, the complete data are given again in tab. 5.2 and tab. 5.3.

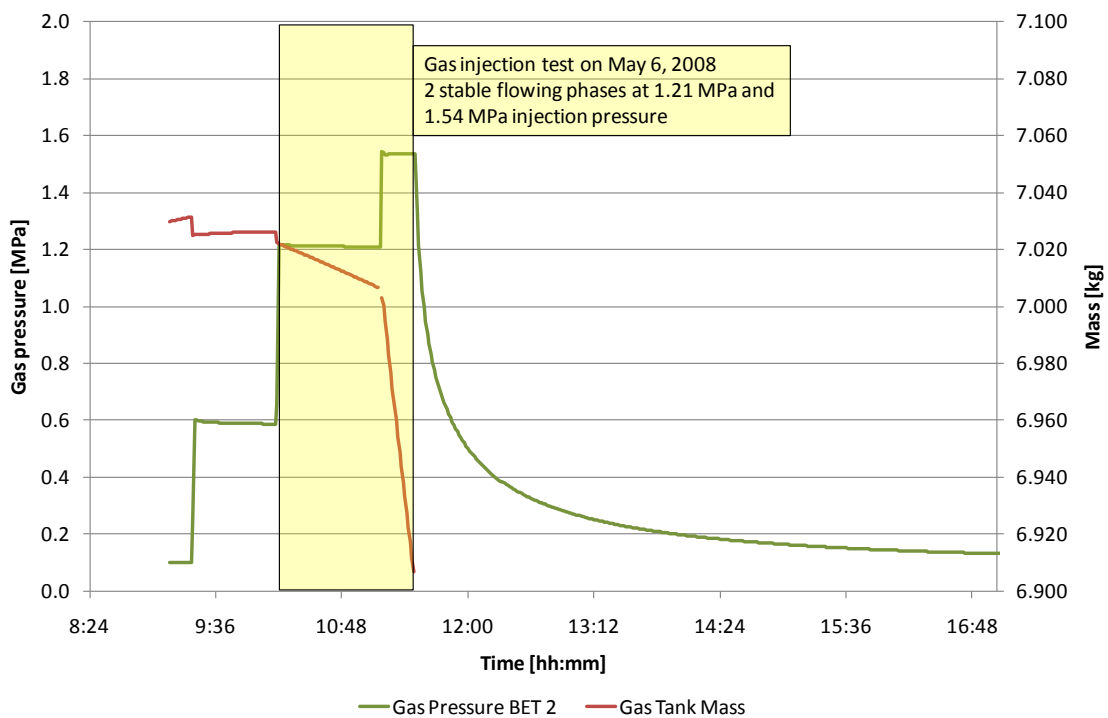


Fig. 5.5 Gas injection BET 2 in May 2008: Gas injection pressure and gas tank mass

In addition to the tests at BET 2 and BET 5 first gas injection tests were performed at BET 4, BET 6, and BET 1.

At BET 4 gas entry was observed at 1.7 MPa, and several stable flowing phases at increasing injection pressure were realised. At BET 6, no gas entry could be achieved at pressures up to 3.6 MPa.

The first pressure step of 0.6 MPa at BET 1 resulted in an anomalous gas flow into the formation (see fig. 5.6). Gas flow reduced with time, and at the next pressure step of 0.9 MPa no gas flow was detected at all. Reason for this anomaly is the fact that BET 1 had never been re-saturated. The first pressure step results in gas filling the pores close to the borehole wall, and the flow reduces as gas pressure in the open pores increases. New pore space by dilatant opening is, however, only created at higher pressures above 1.2 MPa when stable flowing phases can be detected (see fig. 5.6).

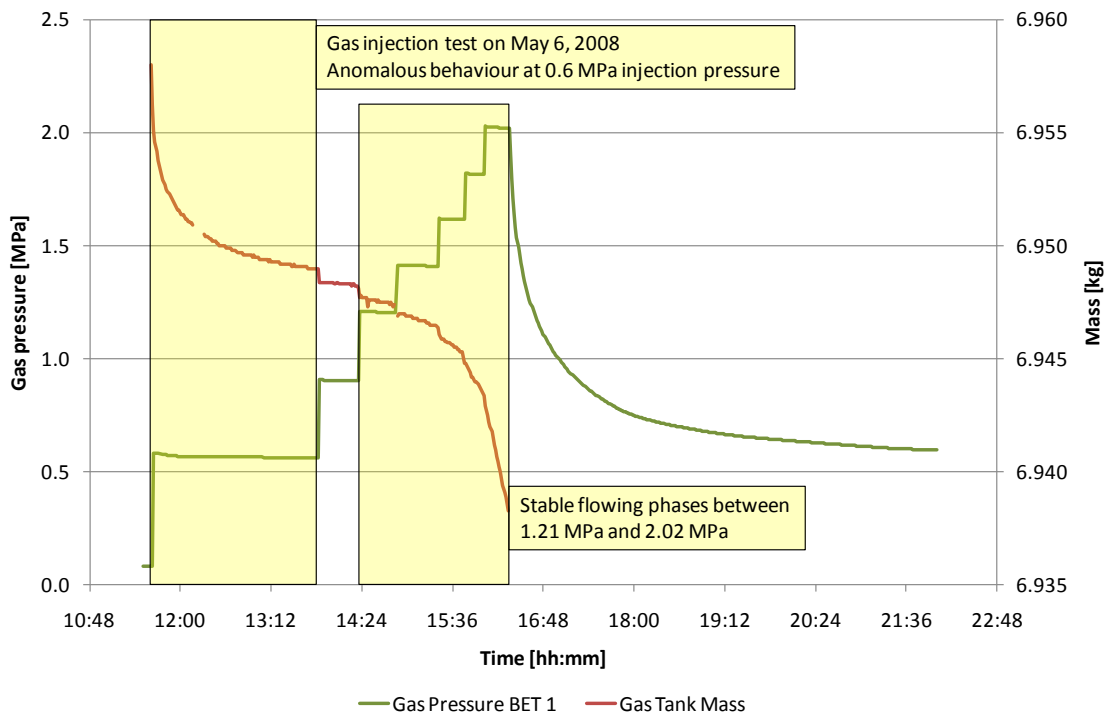


Fig. 5.6 Gas injection BET 1 in May 2008: Gas injection pressure and gas tank mass

5.1.5 Water injection tests May/June 2008

After completion of the gas injection tests in May 2008 the test intervals were re-saturated, and water permeability tests were performed. The results showed a higher scatter and mostly lower values than during the first water injection test (see tab. 5.1); BET 6 was not evaluable at all. The reason for this is the fact that there is now gas in the system, which means that the assumption of single phase flow in the rock no longer

holds. The permeability obtained is an effective permeability at an unknown saturation state.

Tab. 5.1 Results of water permeability testing (values with an asterisk (*)) not reliable due to gas in the system

	Water Permeability [m ²]		
	August 2007	June 2008	September 2009
BET 1	$2 \cdot 10^{-16}$ (*)	$3 \cdot 10^{-17}$ (*)	$4 \cdot 10^{-18}$ (*)
BET 2	$4 \cdot 10^{-19}$	$1 \cdot 10^{-18}$ (*)	$2 \cdot 10^{-18}$
BET 3	$5 \cdot 10^{-19}$	$1 \cdot 10^{-22}$ (*)	$9 \cdot 10^{-21}$
BET 4	$5 \cdot 10^{-19}$	$1 \cdot 10^{-19}$ (*)	$2 \cdot 10^{-19}$
BET 5	$1 \cdot 10^{-19}$	$1 \cdot 10^{-21}$ (*)	$1 \cdot 10^{-19}$
BET 6	$2 \cdot 10^{-20}$		$2.5 \cdot 10^{-21}$
BMB 3			$4 \cdot 10^{-19}$
BMB 4			$8 \cdot 10^{-21}$

5.1.6 Water injection tests September 2009

Between June 2008 and September 2009 the in-situ activities were paused. The gas was allowed to dissipate and the rock to re-saturate. In September 2009 a new series of water injection tests was performed. The results are shown in tab. 5.1. The values scatter less than in June 2008 and are closer to the originally measured ones.

Additional tests were performed at BMB 3 and BMB 4. The obtained water permeabilities are in the range of the values measured in the BET boreholes.

5.1.7 Gas injection tests December 2009

In December 2009 a last series of gas injection tests was started. This time, it was successfully attempted to obtain stable gas flowing phases not only with increasing pressure steps, but also after reducing pressure to lower values. The procedure is illustrated in fig. 5.7 for the injection test at BET 5. Stable flowing phases can be

recognized at 2.2 MPa, 2.4 MPa, and 2.9 MPa gas pressure, but also at 2 MPa after reducing the pressure. Since there is already gas in the system and an opening of pathways has occurred, gas continues flowing at a pressure below the entry pressure of 2.2 MPa.

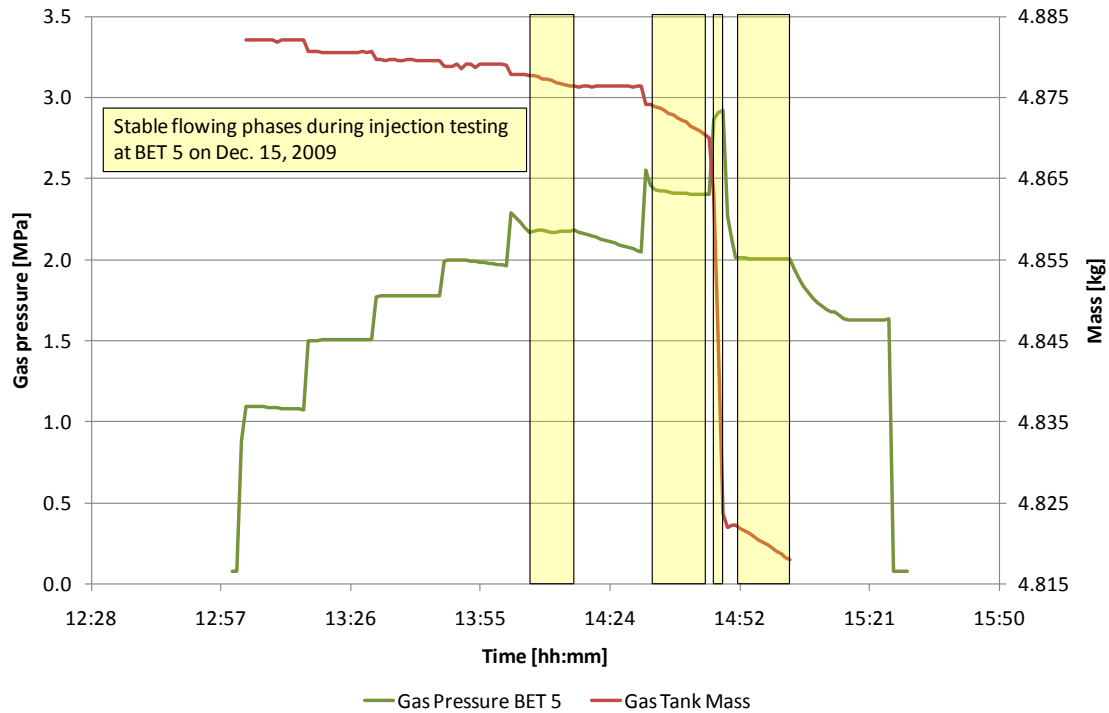


Fig. 5.7 Gas injection BET 5 in December 2009: Gas injection pressure and gas tank mass

Figure 5.8 shows the measurement data of BET 3. Here, gas was injected for the first time. The behaviour of BET 3 is quite close to that of BET 5, although the gas entry pressure is somewhat higher (3.2 MPa). At BET 6, again no gas entry could be achieved, although the injection pressure was increased to 5 MPa.

Gas injection at BET 1 first resulted in no flow, until at 3 MPa injection pressure a gas-frac occurred, marked by a sudden high flow rate which emptied the gas tank within seconds. Since BET 1 is the unsaturated test interval, this behaviour was not expected, given the gas entry pressure of 1.2 MPa measured in May 2008. The incident can only be explained by assuming that the injection tube was blocked (as the return tube had been blocked all the time) and was cleared only at 3 MPa gas pressure, which then led to the fracturing.

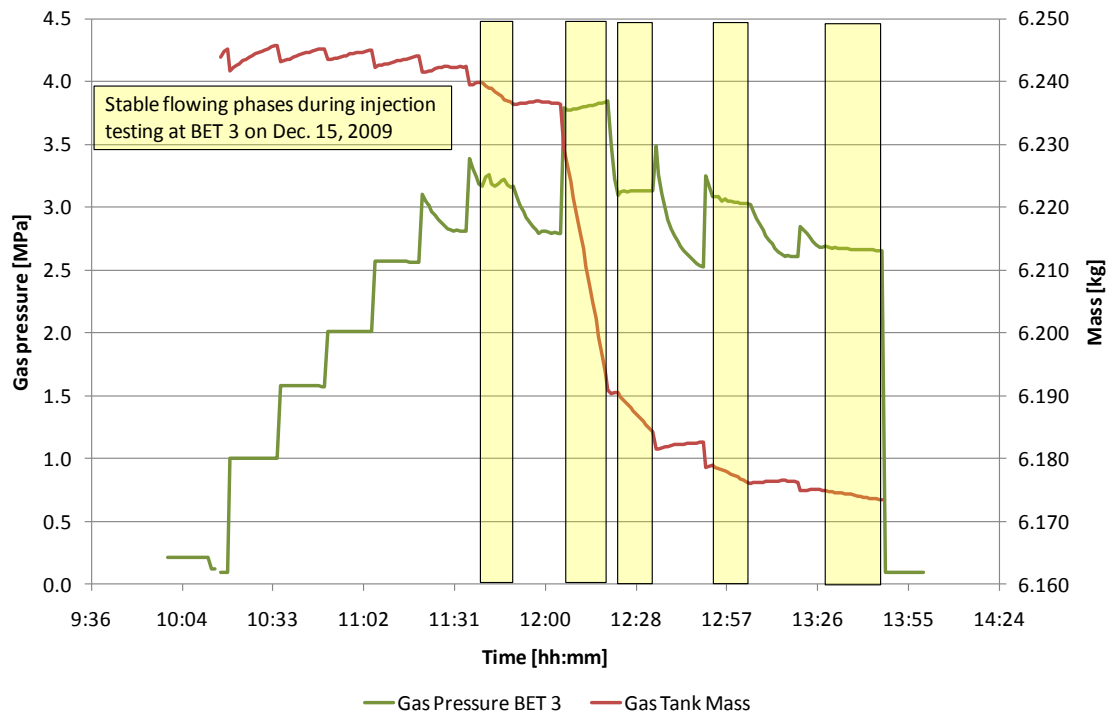


Fig. 5.8 Gas injection BET 3 in December 2009: Gas injection pressure and gas tank mass

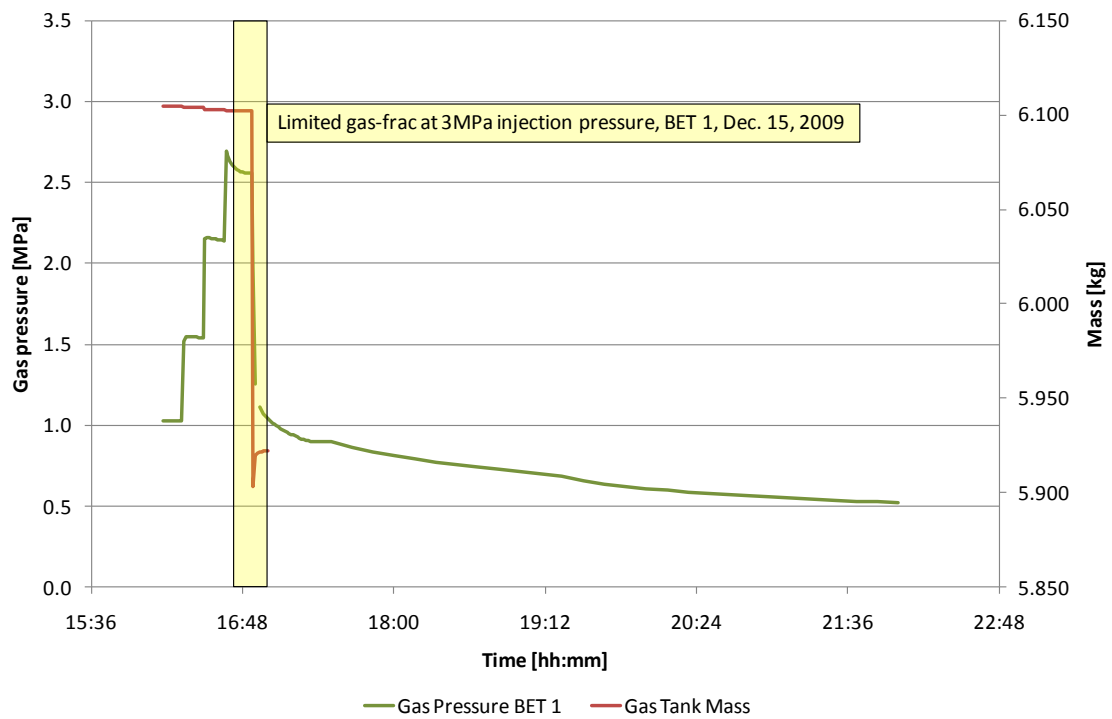


Fig. 5.9 Gas injection BET 1 in December 2009: Gas injection pressure and gas tank mass

The gas-frac was, however, limited, since after closing of the injection valve the pressure remained at about 1 MPa and reduced very slowly afterwards.

Gas injection tests were also performed at the boreholes BMB 3 and BMB 4. For both boreholes a gas entry pressure of about 2 MPa was found, and stable flowing phases were evaluated both with increasing and decreasing pressure steps. The measurement curves of BMB 3 are shown in fig. 5.10 as an example.

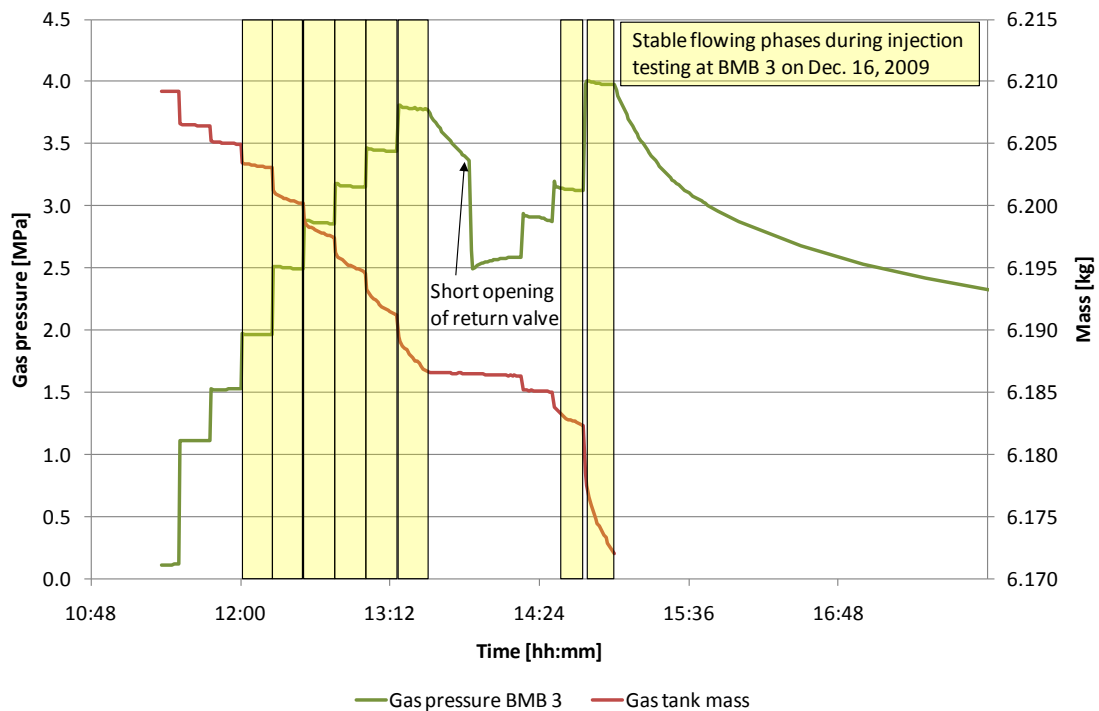


Fig. 5.10 Gas injection BMB 3 in December 2009: Gas injection pressure and gas tank mass

All the gas entry pressures determined during the various gas injection campaigns are compiled in tab. 5.2. The table shows that values around 2 MPa seem to be typical for the gas entry pressure. After gas injection without subsequent re-saturation the entry pressures remained lower (BET 2 and BET 5); after re-saturation and a longer resting period, however, the original values were nearly restored.

Tab. 5.2 Gas entry pressures (gas frac at BET 1 is marked with an asterisk (*))

	Gas Entry Pressure [MPa]		
	November 2007	May 2008	December 2009
BET 1		1.2	3.0 (*)
BET 2	1.8	1.2	1.6
BET 3			3.2
BET 4		1.7	2.45
BET 5	2.4	1.8	2.2
BET 6			>5.0
BMB 3			1.97
BMB 4			1.97

The apparent gas permeabilities evaluated from the stable flowing phases during the various gas injection campaigns are compiled in tab. 5.3 for the BET boreholes. The table shows a pronounced dependence of the apparent gas permeability on the injection pressure. When reducing the injection pressure, the gas permeability remains higher than at the corresponding pressure during pressure increase, because gas is already in the system and pathways have been produced.

The gas permeabilities after the re-saturation and resting period measured in December 2009 are generally lower than those from May 2008 for corresponding injection pressures, which is in agreement with the recovery of the gas entry pressures.

For the BMB boreholes, the dependence of apparent gas permeability on the injection pressure is much less pronounced, as can be taken from tab. 5.4.

Tab. 5.3 Apparent gas permeabilities for the BET boreholes

	November 2007		May 2008		December 2009			
	Injection Pressure [MPa]	Apparent Gas Permeability [m ²]	Injection Pressure [MPa]	Apparent Gas Permeability [m ²]	Injection Pressure [MPa]	Apparent Gas Permeability [m ²]		
BET 1			1.21	$3.1 \cdot 10^{-19}$	3.00	$9.4 \cdot 10^{-16}$		
			1.41	$3.4 \cdot 10^{-19}$				
			1.62	$1.1 \cdot 10^{-18}$				
			1.82	$1.2 \cdot 10^{-18}$				
			2.02	$2.7 \cdot 10^{-18}$				
BET 2	1.80	$7.9 \cdot 10^{-16}$	1.21	$7.9 \cdot 10^{-18}$	1.65	$1.0 \cdot 10^{-18}$		
			1.54	$9.6 \cdot 10^{-17}$				
	0.49	$5.1 \cdot 10^{-18}$					1.91	$5.5 \cdot 10^{-18}$
	0.99	$8.5 \cdot 10^{-18}$					1.34	$2.1 \cdot 10^{-18}$
	1.50	$2.2 \cdot 10^{-17}$					1.13	$1.4 \cdot 10^{-18}$
	1.60	$2.0 \cdot 10^{-16}$						
BET 3					3.20	$1.5 \cdot 10^{-18}$		
					3.80	$8.1 \cdot 10^{-18}$		
					3.13	$2.5 \cdot 10^{-18}$		
					3.05	$1.1 \cdot 10^{-18}$		
					2.67	$5.1 \cdot 10^{-19}$		
BET 4			1.76	$4.8 \cdot 10^{-18}$	2.45	$4.4 \cdot 10^{-19}$		
			2.10	$2.5 \cdot 10^{-17}$	2.81	$1.5 \cdot 10^{-18}$		
			2.38	$7.6 \cdot 10^{-17}$	1.85	$2.6 \cdot 10^{-19}$		
BET 5	2.40	$5.7 \cdot 10^{-19}$	1.86	$1.6 \cdot 10^{-17}$	2.20	$1.1 \cdot 10^{-18}$		
	2.70	$1.3 \cdot 10^{-17}$			2.41	$2.4 \cdot 10^{-18}$		
	2.95	$1.1 \cdot 10^{-16}$			2.90	$9.9 \cdot 10^{-17}$		
					2.00	$3.7 \cdot 10^{-18}$		
BET 6								

Tab. 5.4 Apparent gas permeabilities for BMB 3 and BMB 4

	December 2009	
	Injection Pressure [MPa]	Apparent Gas Permeability [m ²]
BMB 3	1.97	$5.0 \cdot 10^{-19}$
	2.50	$7.8 \cdot 10^{-19}$
	2.87	$7.7 \cdot 10^{-19}$
	3.16	$7.8 \cdot 10^{-19}$
	3.45	$8.6 \cdot 10^{-19}$
	3.78	$9.5 \cdot 10^{-19}$
	3.13	$7.5 \cdot 10^{-19}$
	3.98	$1.5 \cdot 10^{-18}$
BMB 4	1.97	$7.5 \cdot 10^{-19}$
	2.51	$9.3 \cdot 10^{-19}$
	2.98	$6.0 \cdot 10^{-19}$
	3.27	$3.6 \cdot 10^{-19}$
	3.55	$1.2 \cdot 10^{-18}$
	3.93	$2.3 \cdot 10^{-18}$
	2.94	$6.1 \cdot 10^{-18}$

5.2 Laboratory testing

5.2.1 Small samples

The laboratory tests for investigation of gas pressure induced damage and re-compaction were started by determining the gas permeability of four samples from the core section between 6.24 m and 7.22 m at different isostatic loads of 2.4 MPa and 7.5 MPa. Gas pressure was applied via axial boreholes in the core centres. The measurements showed no systematic dependence of gas permeability on the external load under the applied conditions.

A control measurement showed that the measured flow rates were corrupted by gas release from the hydraulic oil used for applying the load. The load is generated by pressing the oil with nitrogen in an autoclave. Apparently, nitrogen was dissolved in the

oil and later released at the rubber jacket around sand-filled annulus, thus increasing the measured gas flow rate.

Since the first tests had shown no dependence of the permeability on the load, further measurements were only performed with the maximum pressure of 8 MPa, while ascertaining that no additional gas flow into the annulus was possible. The gas permeabilities determined in that way were in the range of 10^{-22} m^2 to 10^{-20} m^2 .

Subsequently, first damage tests were started at a load of 3 MPa. Gas was injected via the central borehole and the injection pressure was slowly raised. At a pressure of 1.2 MPa one of the samples showed a relatively fast pressure decay within 3.4 h, which can be attributed to the opening of pathways.

For investigating the behaviour after gas break-through nitrogen was injected into a radially loaded sample (load was 8.0 MPa). When gas break-through was detected at an injection pressure of 8.9 MPa, the injection was stopped and the further evolution was monitored. After several hours to days a new gas flow occurred and pressure reduced. This behaviour repeated in several time intervals, until a pressure of about 4 MPa was reached. This observation hints to a more or less continuous closing of pathways. In a last step of this test, the radial load was reduced to 3.5 MPa which is more realistic with respect to the stress conditions in situ. Again, gas flow was observed, and the pressure decreased to 1.5 MPa.

The following tests on the three samples E, F, and G were all performed at 3.5 MPa radial load. Gas injection pressure was increased stepwise with about one week duration per pressure step. For sample E, a significant gas flow was detected only at 6 MPa injection pressure. Subsequently the pressure continuously decreased to 1.8 MPa, in contrast to the first sample where the pressure decreased more stepwise.

After waiting for two weeks two new injection tests were performed, which showed significant gas flow already at 2.6 MPa and 2.8 MPa, respectively – an observation that agrees with the in-situ results.

The tests with the samples F and G were performed in the same way. Sample F showed gas flow already at test start-up, while Sample G behaved more like sample E. Here, a gas flow was detected only at 2.5 MPa injection pressure. The injection phase

was followed by a shut-in phase with pressure decay. Several of these cycles were conducted.

The experiments showed that permeability and flow rates are strongly dependent on injection pressure. Increasing injection pressures below the radial load led to moderate permeability increase, which accelerated when injection pressure approached the external load. Exceeding the external load resulted in a permeability and flow rate jump, it could, however, been shown that this was an artificial result of the test configuration.

The measurement results with injection pressure below the external load clearly hint to an opening and closing of pathways. Since the process was relatively slow and showed no sudden permeability changes, the assumption of a dilatant pathway opening and closing seems reasonable.

The permeabilities recorded below external load range between 10^{-19} m^2 and 10^{-21} m^2 for sample F (see fig. 5.11). The permeabilities obtained during the second injection cycle after the shut-in phase are somewhat higher than during the first cycle, which shows that the pathways have not completely closed in the meantime. This agrees well with the in-situ results (see section 5.1).

Sample G shows a similar behaviour as sample F, although gas flow was only detected at an injection pressure of 2.5 MPa, with a gas permeability of 10^{-21} m^2 (fig. 5.12). Surprisingly, after the shut-in phase and new increase of the injection pressure no gas flow could be observed at first. Figure 5.12 shows this as a permeability drop. After further raising the gas pressure a pronounced permeability increase was found. This behaviour of the sample is not completely clear, it has to be a reaction to the pressure increase, during which a short-term impediment of gas flow must have occurred. The permeabilities evaluated at pressures below the external load ranged between 10^{-19} m^2 und 10^{-23} m^2 .

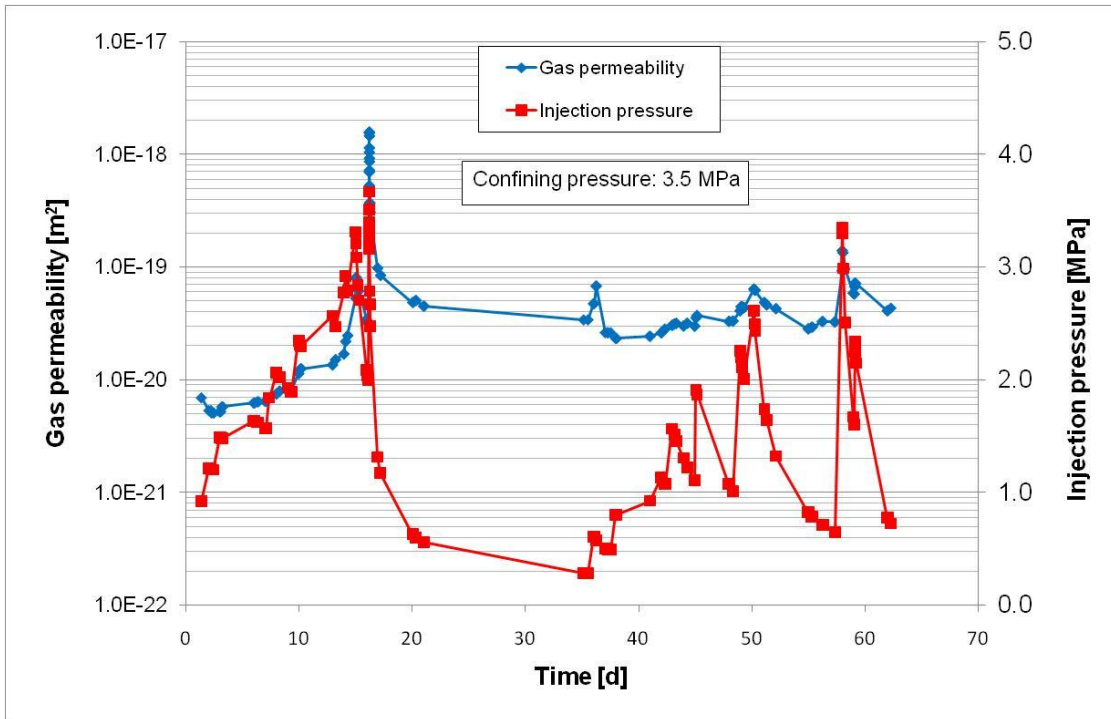


Fig. 5.11 Test history of sample F: Permeability and injection pressure

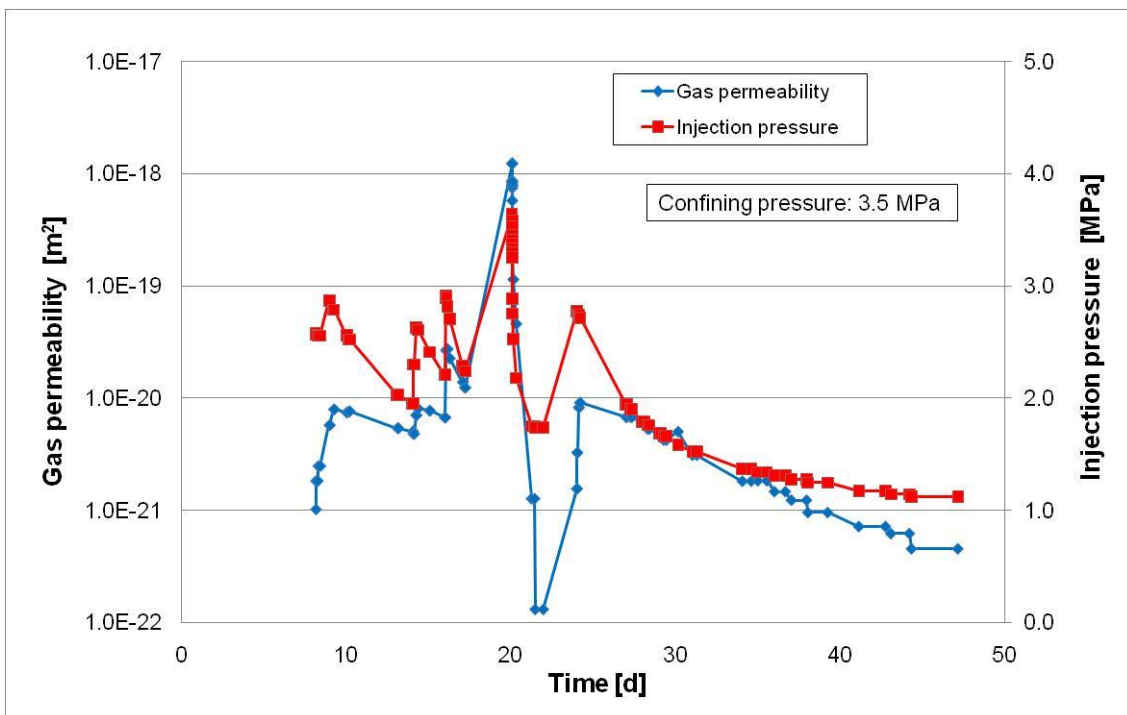


Fig. 5.12 Test history of sample G: Permeability and injection pressure

In order to check the results of the investigations with isostatically loaded samples with respect to possible influences of the test configuration, additional measurements were

performed with a sample in a triaxial cell (sample 2). Radial load was set to 3.5 MPa, and axial load ranged between 4 MPa and 5 MPa. Applying the axial load to the samples resulted in a reduction of permeability from about 10^{-18} m^2 to 10^{-19} m^2 .

Although the isostatic tests in the autoclave showed artifacts when injection pressure exceeded the external load, the triaxial tests with independent radial and axial load confirmed the results obtained for gas pressures below the external load. At an injection pressure of 2 MPa an increase in gas permeability was measured. Permeability reached values of 10^{-17} m^2 . Reducing the injection pressure and increasing it again led to a decrease and subsequent increase of permeability (see fig. 5.13).

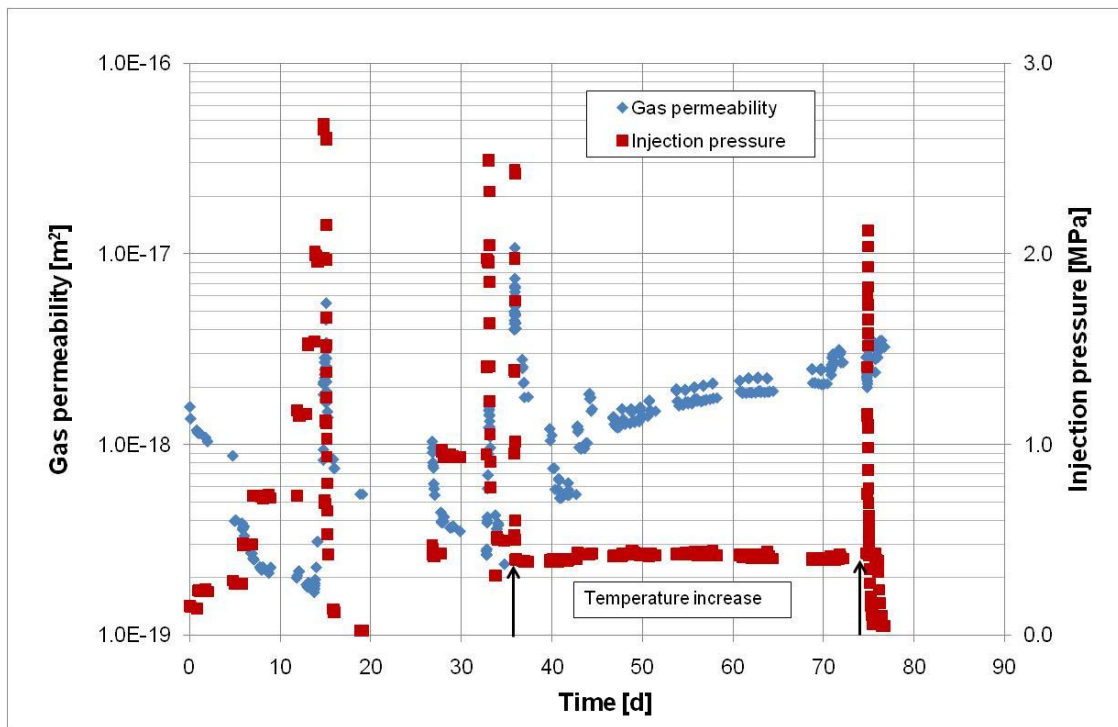


Fig. 5.13 Test history of sample 2: Permeability and injection pressure

In order to investigate the influence of temperature on the gas transport behaviour the test was continued under isostatic load and elevated temperature up to 90 °C. Starting at a temperature of 50 °C a water release from the sample was observed, while the gas permeability increased. This can be explained by the displacement of water, increasing the pore space available for gas transport. When decreasing the temperature again, the water release stops (fig. 5.14).

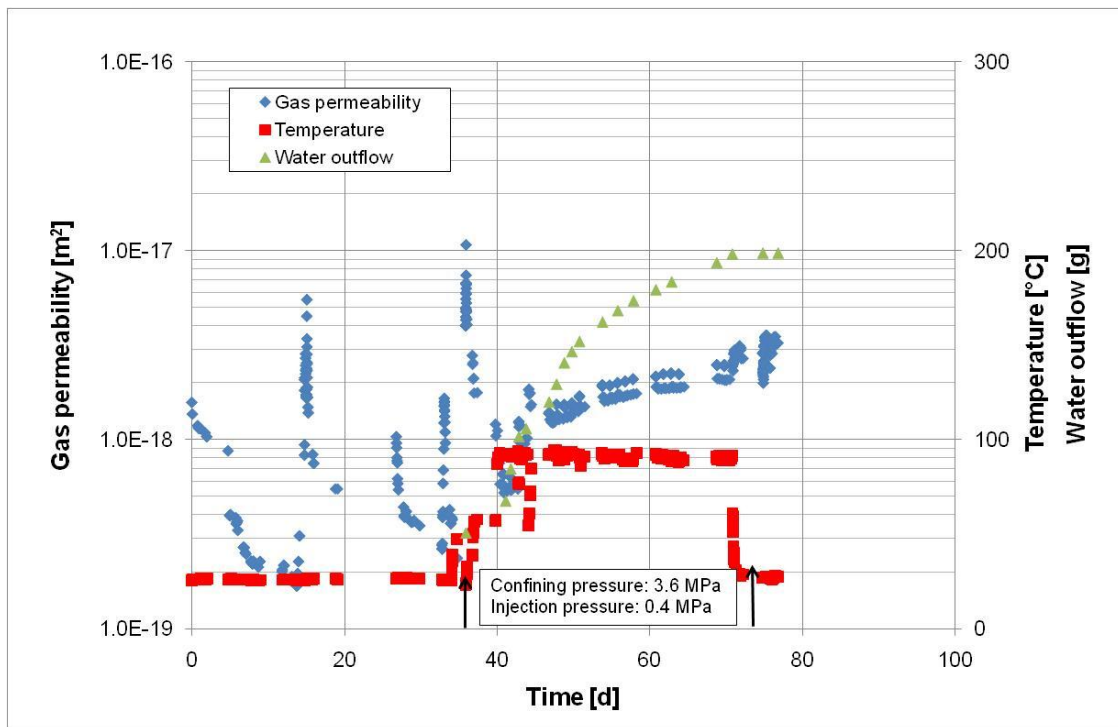


Fig. 5.14 Test history of sample 2: Permeability and water release at elevated temperature

A second test for the investigation of the temperature influence was performed under constant load and constant injection pressure (sample 3, see fig. 5.15). A reduction of gas permeability at the beginning of the test can be explained by thermally induced deformation of the sample. With beginning of water release gas permeability increases again.

During the test the temperature control unit failed. After restart of the test a large jump in gas permeability can be observed which is probably due to thermal damage of the sample as a consequence of the rapid cool-down from 90 °C to ambient temperature. Water release rises again with temperature increase.

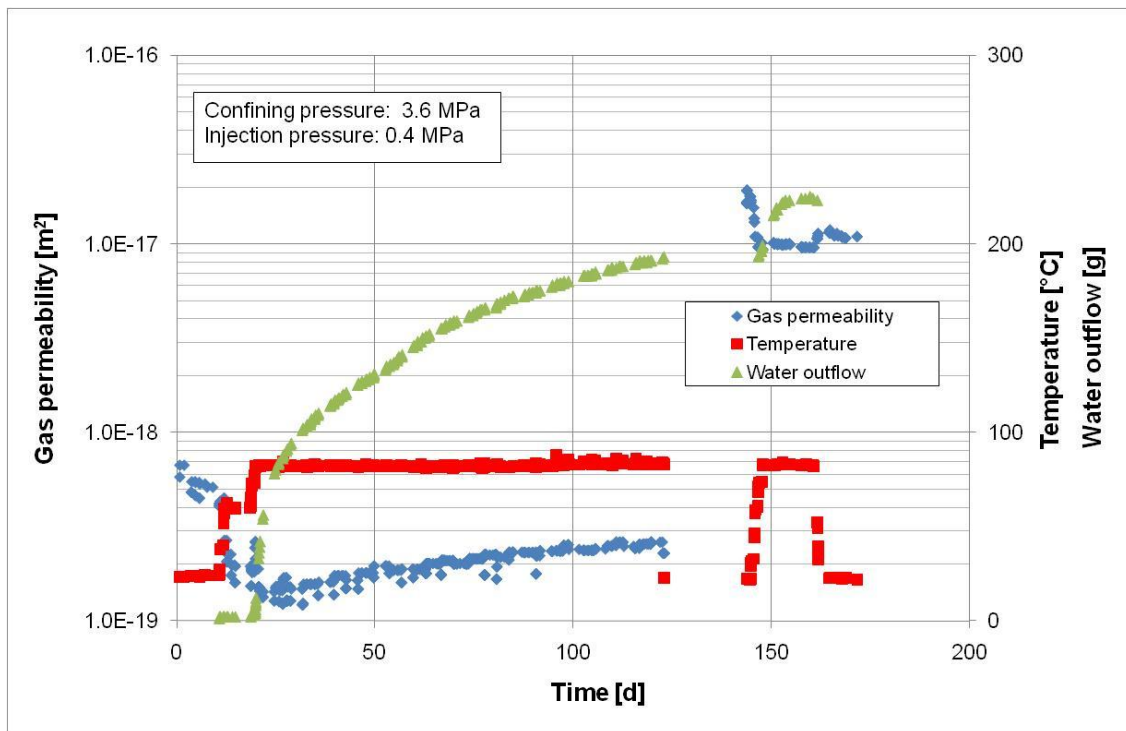


Fig. 5.15 Test history of sample 2: Permeability and water release at elevated temperature

5.2.2 Large samples

The first tests with a large sample were performed with the damaged sample 2L. It had been planned to apply a load of 4.5 MPa, but when, at a load of 3 MPa, a significant axial deformation was observed, this axial load was kept by deformation control. The radial load was set to 3.5 MPa. The following investigations showed that the failure plane had a significant influence on the sample behaviour.

A relatively high gas flow rate occurred already at injection pressures between 0.5 MPa and 0.8 MPa. When starting the test, a qualitative gas permeability increase from about 10^{-15} m^2 to 10^{-14} m^2 at 0.46 MPa injection pressure (see fig. 5.16). Then, however, permeability decreased to $3 \cdot 10^{-15} \text{ m}^2$ when gas pressure further increased. This may be an effect of swelling, caused by the water supplied via the wetted nitrogen, which resulted in a partial closing of pathways.

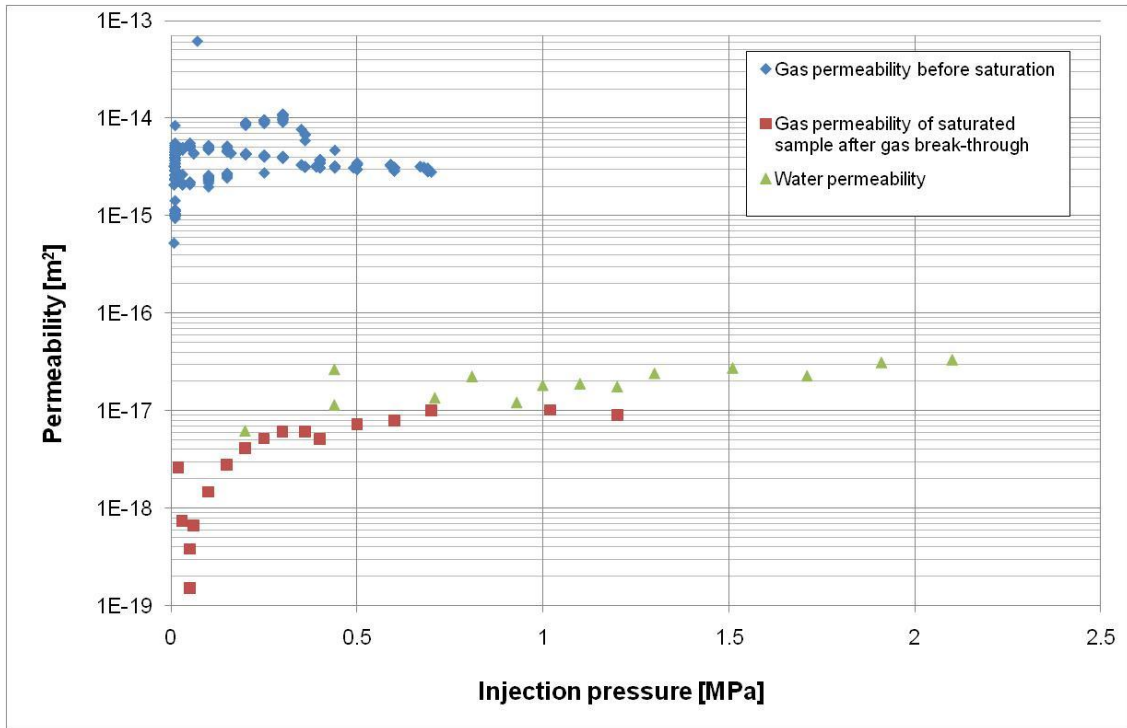


Fig. 5.16 Comparison of the gas permeabilities before saturation and after gas break-through and the water permeability (damaged sample 2L)

Since very high flow rates were reached already at low injection pressures, further tests with injection of Pearson water were added, in order to see whether a partial healing by swelling could be reached. After re-saturation of the sample the water permeability was determined at an injection pressure of 0.2 MPa and yielded a value of $6.2 \cdot 10^{-18} \text{ m}^2$, considerably lower than the originally measured gas permeabilities. Increasing the injection pressure to 2.1 MPa resulted in a water permeability increase to $3.3 \cdot 10^{-17} \text{ m}^2$ (fig. 5.16), which again hints to pathway dilation.

After finishing the water permeability tests, gas was injected and a break-through pressure of 0.4 MPa was obtained. After gas break-through, the injection pressure was reduced to 0.02 MPa in order to limit water release. The permeability was then determined as $2.6 \cdot 10^{-18} \text{ m}^2$, three orders of magnitude lower than the original gas permeability.

Afterwards, injection pressure was continuously increased and the permeability evaluated (see fig. 5.16). The comparison to the gas permeability values before re-saturation shows that after re-saturation gas permeability never reaches the original values, which is caused by swelling on the one hand and by the reduction of available pore space due to water uptake on the other hand. The increase of gas permeability

with increasing injection pressure can be caused by pathway dilation, but also by water displacement from the sample (de-saturation), because water was released during the gas flow process.

Figure 5.17 shows the temporal evolution of gas permeability after break-through with the injection pressure. Permeability directly reacts on changes in injection pressure. After decreasing the injection pressure, a new short-term increase to 1.2 MPa does not lead to permeability increases above 10^{-17} m^2 .

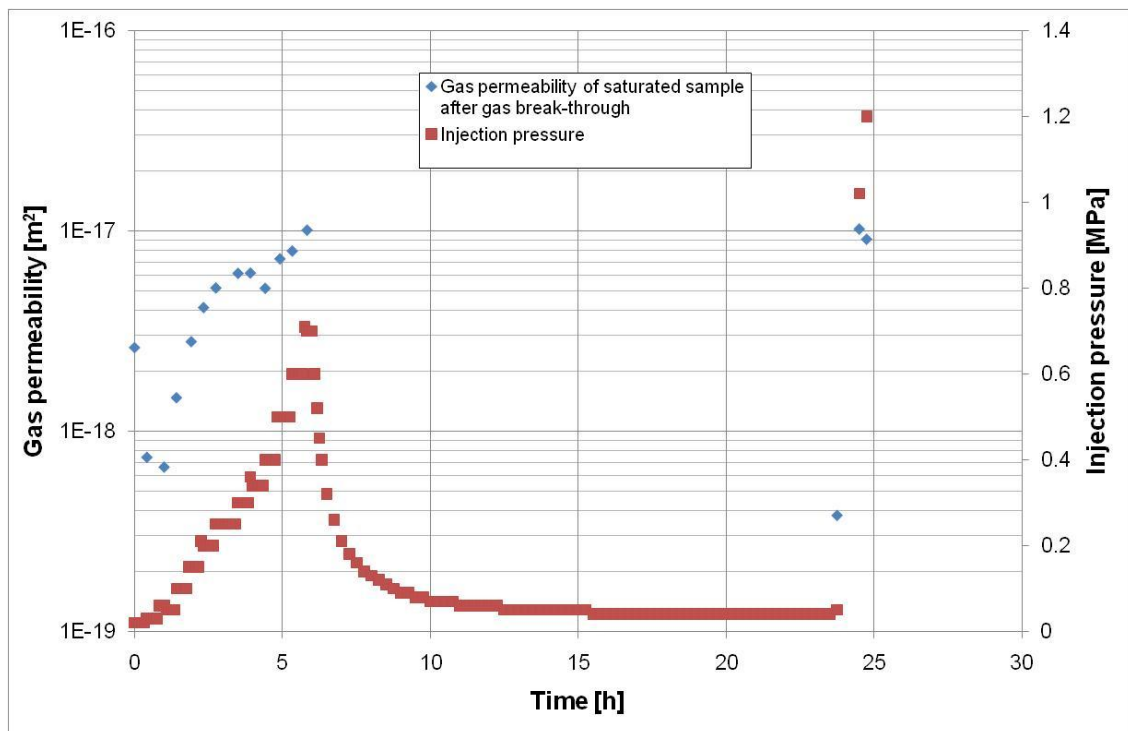


Fig. 5.17 Evolution of gas permeability with time after gas break-through at different gas injection pressures (sample 2L)

After finishing the tests with the damaged sample 2L, a similar experiment was performed using the intact sample 3L.

The originally planned load conditions could be applied on sample 3L: Axial load was 4.5 MPa, radial load was 3.5 MPa. The initial permeability was determined by gas injection via the axial borehole with an injection pressure of 0.04 MPa and led to a value of $4.3 \cdot 10^{-18} \text{ m}^2$. With increasing injection pressure permeability rose to $2 \cdot 10^{-16} \text{ m}^2$ at 3 MPa. Repeating the measurement after four days resulted in a similar behaviour, although the start value, which was also determined at 0.04 MPa injection pressure, was already somewhat higher ($1.2 \cdot 10^{-17} \text{ m}^2$). The end value at 3 MPa injection

pressure was with $1.5 \cdot 10^{-16} \text{ m}^2$ slightly lower than during the first measurement (see figs. 5.18 and 5.19). Again, it can be deduced that gas injection did not result in permanent damage of the sample.

After finishing the gas injection tests the sample was re-saturated with Pearson water. Over a time period of 57 days no water release from the outer surface of the sample could be detected. Finally, a new gas injection cycle was started. It was assumed that the sample was saturated with water at least close to the central injection borehole, so that gas injection would give a reliable value for the gas entry pressure. Gas injection pressure was continuously increased, until a significant gas flow through the sample was detected (figs. 5.18 and 5.19). The gas permeabilities below 10^{-20} m^2 in the figures are artefacts, caused by gas displacement from the tube system. Gas break-through with a significant flow rate was observed at 3.8 MPa, the respective gas permeability is $1.3 \cdot 10^{-18} \text{ m}^2$. A reduction of injection pressure led again to a reduction of gas permeability to $6 \cdot 10^{-20} \text{ m}^2$.

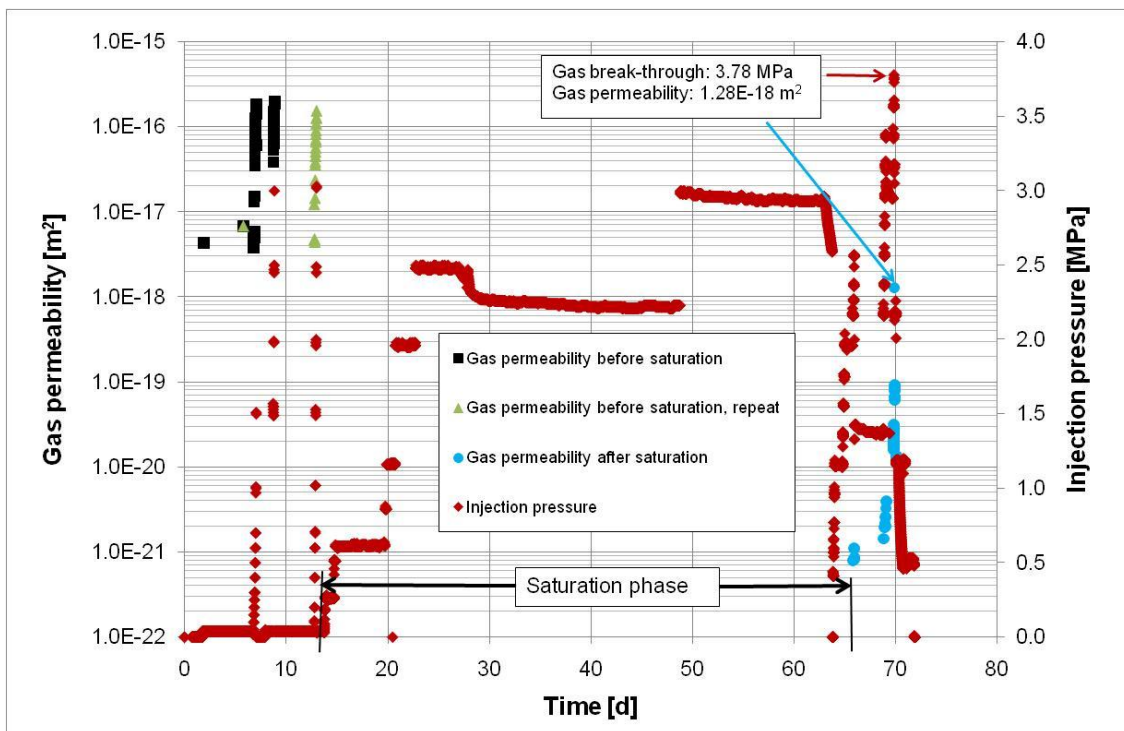


Fig. 5.18 Evolution of gas permeability with time, before and after saturation, at different gas injection pressures (intact sample 3L).

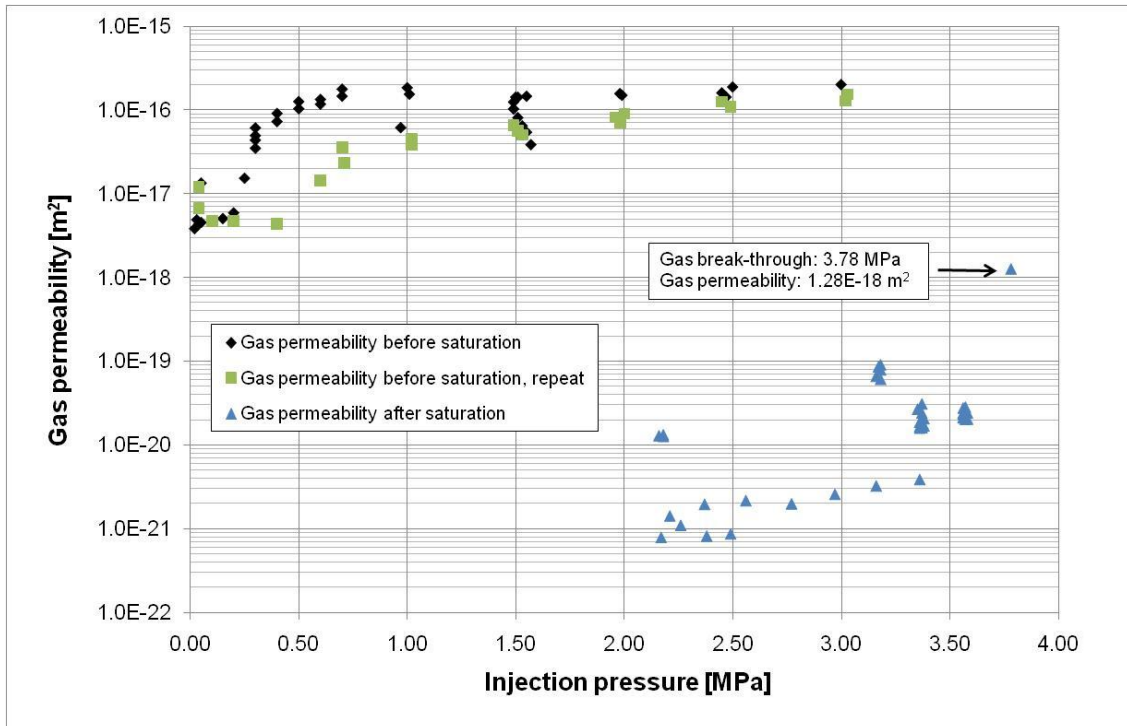


Fig. 5.19 Gas permeability of the intact sample 3L before and after saturation as a function of gas injection pressure (intact sample 3L).

As was already found for the damaged sample, the gas permeability after re-saturation remains far below the values evaluated before re-saturation of the sample (fig. 5.19).

After removing the sample from the apparatus a shear plane was found in the upper third of the sample. The fracture had healed during the re-saturation, so that the upper but could not be removed, even by cautious hammering. Moreover, the low gas permeability after re-saturation and the observation that no water was released during re-saturation confirm that the fracture did not act as an „artificial“ pathway. The sample with the shear plane is shown in fig. 5.20 (left and centre). On the right side of the figure the punched plate that surrounded the sample can be seen, with the mark that was left by the shearing sample.



Fig. 5.20 Removed sample 3L after the end of the test (left: healed shear plane, centre: zoomed in view, right: punched plate with shear mark)

5.2.3 Fracture images

A section of the sample was placed in a rubber jacket, put in the tracer medium, and sealed. Subsequently, it was attempted to press the tracer into the existing fractures by applying an isostatic load of 3 MPa. After curing the sample was inspected under UV light, however, the expected effect was not visible. The tracer medium was only found in the injection borehole and a large fissure. No tracer had entered fine fissures (see fig. 5.21).

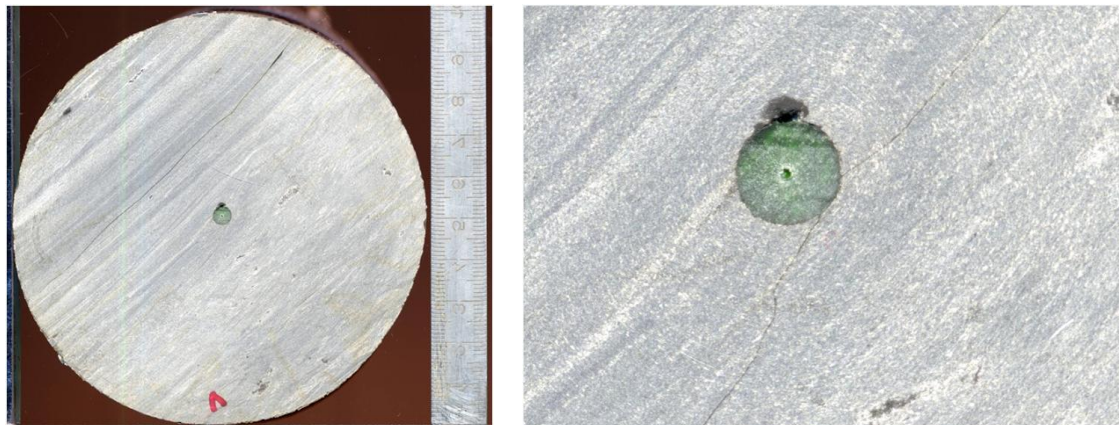


Fig. 5.21 Test for visualisation of fissures by Injection of artificial resin tracers with uranine (left: central borehole with injected tracers; right: detailed view around the central borehole)

Since the fracture visualisation with tracer injection was not successful, a sample was machined down by 2 mm layers and each uncovered layer was scanned with a resolution of 1600 dpi, as described in section 4.2.3. Figure 5.22 shows the digitised

fractures. Only fractures crossing the central borehole are shown, because these are the only that contribute to flow during injection testing. The figure gives a good idea of fracture plane orientation, so this method of fracture visualisation can be considered as successful.

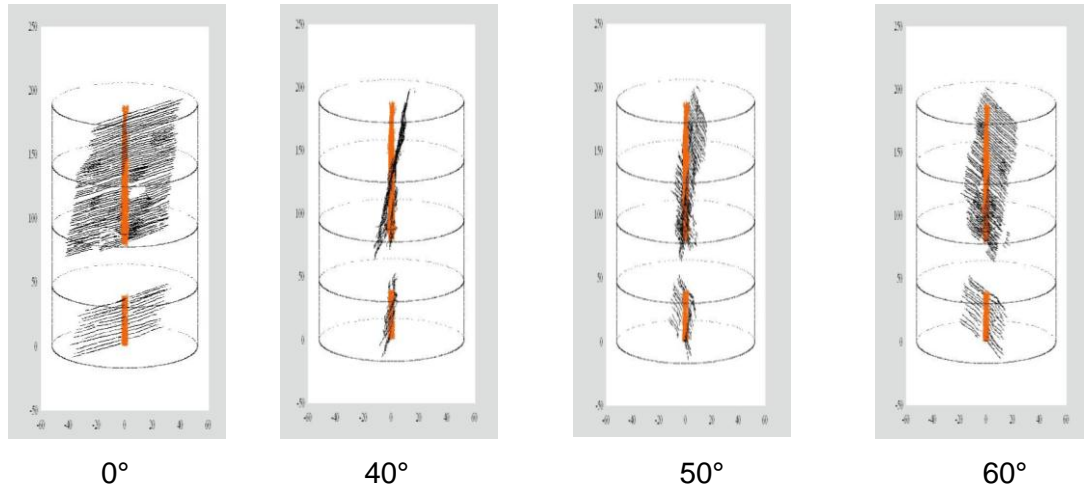


Fig. 5.22 Visualisation of fissures by scanning (only fissures crossing the central borehole)

6 Numerical investigations

To gain experiences with numerical modelling of coupled hydro-mechanical processes in clays, a number of scoping calculations were performed by GRS /ZHA 04/, /ZHA 07/, /ZHA 08/ by using the computer programme CODE_BRIGHT developed by the Geotechnical Engineering Department of the Technical University of Catalonia in Barcelona for analysis of coupled THM phenomena in geological media /UPC 02/.

6.1 Physical modelling

Regarding the tight coupling between fluid flow processes and mechanical deformation in argillaceous rock mass a simplified approach of the recently developed argillite model is used, taking into account the anisotropic primary stress field without any damaging process as well as anisotropic hydraulic and mechanical response in case of 3D modelling. Prior to introducing the results of the numerical simulation a brief description of the formulation and the capabilities of the code used in the analysis as well as the used constitutive model and the depending material parameters are presented.

6.1.1 Theoretical framework

The computer programme CODE_BRIGHT handles coupled thermo-hydro-mechanical problems in porous media. The theoretical framework is composed of three main parts:

- balance equations,
- constitutive equations and
- equilibrium restrictions.

The subscripts identify the phase ('s' for solid, 'l' for liquid and 'g' for gas). The superscripts indicate the species ('h' for mineral, 'w' for water and 'a' for air). The liquid phase may contain water and dissolved air, and the gas phase may be a mixture of dry air and water vapour. Thermal equilibrium between phases is assumed. This means that the three phases are at the same temperature. A general and detailed description is given in /OLI 96/ and in the code manual /UPC 02/, according to the aforementioned literature only a brief description is given in the following section.

6.1.2 Balance equations

The balance equations are established for the porous medium as a whole. The compositional approach is adopted to establish the mass balance equations. It consists of balancing the species rather than the phases. The mass balance of solid present in the medium is written as:

$$\frac{\partial}{\partial t} (\rho_s(1 - n)) + \nabla \cdot (j_s) = 0 \quad (6.1)$$

where ρ_s is the mass of solid per unit volume of solid, j_s is the flux of solid, t is time and ∇ is the divergence operator.

Water is present in liquid and gas phases. The total mass balance of water is expressed as:

$$\frac{\partial}{\partial t} (\theta_l^w S_l n + \theta_g^w S_g n) + \nabla \cdot (j_l^w + j_g^w) = f^w \quad (6.2)$$

where θ_l^w and θ_g^w are the masses of water per unit volume of liquid and gas, respectively. S_α is the volumetric fraction of pore volume, occupied by the alpha phase ($\alpha = l, g$). j_l^w and j_g^w denote the total mass fluxes of water in the liquid and gas phases (water vapour), with respect to a fixed reference system. f^w is an external supply of water per unit volume of medium.

Dry air is present in liquid and gas phases. The total mass balance of dry air is expressed as:

$$\frac{\partial}{\partial t} (\theta_l^a S_l n + \theta_g^a S_g n) + \nabla \cdot (j_l^a + j_g^a) = f^a \quad (6.3)$$

where θ_l^a and θ_g^a are the masses of dry air per unit volume of liquid and gas, respectively. S_α is the volumetric fraction of pore volume, occupied by the alpha phase ($\alpha = l, g$). j_l^a and j_g^a denote the total mass fluxes of dry air in the liquid and gas phases (water vapour), with respect to a fixed reference system. f^a is an external supply of dry air per unit volume of medium.

Thermal equilibrium between phases is assumed. This means that the three phases are at the same temperature. Consequently, the total internal energy, per unit volume

of porous media, is obtained adding the internal energy of each phase. Applying the balance equation to this quantity, the following equation is obtained:

$$\frac{\partial}{\partial t} (E_s \rho_s (1 - \phi) + E_l \rho_l S_l \phi + E_g \rho_g S_g \phi) + \nabla \cdot (\mathbf{j}_c + \mathbf{j}_{Es} + \mathbf{j}_{El} + \mathbf{j}_{Eg}) = f^E \quad (6.4)$$

where E_s is the solid specific internal energy; E_l and E_g are specific internal energies corresponding to liquid and gas phase, respectively, ρ_s is the solid density; ρ_l and ρ_g are the liquid and gas phase densities; \mathbf{j}_c is the conductive heat flux; \mathbf{j}_{Es} is the advective energy flux of solid phase with respect to a fixed reference system; \mathbf{j}_{El} and \mathbf{j}_{Eg} are the advective energy flux of liquid and gas phases, respectively, with respect to a fixed reference system; f^E is the energy supply per unit volume of medium.

The balance of momentum for the porous medium reduces to the equilibrium equation in total stresses:

$$\nabla \cdot \boldsymbol{\sigma} + \mathbf{b} = 0 \quad (6.5)$$

where $\boldsymbol{\sigma}$ is the stress tensor and \mathbf{b} is the vector of body forces.

6.1.3 Equilibrium restrictions

Equilibrium restrictions are given for the concentration of water vapour in gas and of dissolved air in water. The mass of water vapour per unit volume of gas (θ_g^w) is determined via the psychrometric law:

$$\theta_g^w = (\theta_g^w)^0 \exp \left[\frac{-(P_g - P_l) M_w}{R(273.15 + T) \rho_l} \right] \quad (6.6)$$

where P_l and P_g are liquid and gas pressures, respectively, $(\theta_g^w)^0$ is the vapour density in the gaseous phase in contact with a planar surface (i.e. when $P_g - P_l = 0$), M_w is the molecular mass of water (0.018 kg/mol), R is the gas constant (8.314 J/mol·K) and T is the temperature (in degree Celsius). $(\theta_g^w)^0$ is depending on temperature. The vapour partial pressure is computed by means of the ideal gas law.

The solubility of air in water is controlled by Henry's law:

$$\omega_1^g = \frac{P_a}{H} \cdot \frac{M_a}{M_w} \quad (6.7)$$

where ω_1^g is the mass fraction of air in the liquid, P_a is the partial pressure of air, M_a is the molecular mass of air (0.02895 kg/mol) and $H = 10000$ MPa is Henry's constant. According to the definition of partial density, $\theta_1^w = \omega_1^g \cdot \rho_l$.

6.1.4 Constitutive equations

The constitutive equations establish the link between the independent variables and the dependent variables. Concerning the hydraulic problem it is assumed that the liquid and gas flows follow Darcy's law:

$$q_\alpha = -K_\alpha(\nabla P_\alpha - \rho_\alpha \mathbf{g}) \quad (6.8)$$

where $K_\alpha = \mathbf{k} k_{r\alpha} / \mu_\alpha$ is the permeability tensor. The intrinsic permeability tensor (\mathbf{k}) depends on the pore structure of the porous medium. $k_{r\alpha}$ is the value of relative permeability that controls the variation of permeability in the unsaturated regime and μ_α denotes the dynamic viscosity. α stands either for l or g depending on whether liquid or gas flow is considered. \mathbf{g} is the gravity vector. The variation of intrinsic permeability with porosity is given by:

$$k = \mathbf{k}_0 \cdot \frac{\phi^3}{(1-\phi)^2} \cdot \frac{(1-\phi_0)^2}{\phi_0^3} \quad (6.9)$$

where ϕ_0 is a reference porosity. The relative permeabilities of the liquid and gaseous phases are dependent on the degree of liquid saturation according to:

$$S_e = \frac{S_l - S_{lr}}{S_{ls} - S_{lr}} \quad (6.10)$$

and

$$k_{rl} = A \cdot S_e^\lambda \quad (6.11a)$$

$$k_{rg} = 1 - k_{rl} \quad (6.11b)$$

where S_l , S_{lr} , S_{ls} , S_e are the actual, residual, maximum and effective saturation of liquid, respectively, and A and λ are parameters.

It is necessary to define the retention curve of the materials relating to the degree of saturation to suction ($P_g - P_l$). The expression of Van Genuchten is selected:

$$S_e = \left[1 + \left(\frac{P_g - P_l}{P} \right)^{1/(1-\beta)} \right]^{-\beta} \quad (6.12)$$

where $P_g - P_l \geq 0$ and $P = P_0 \cdot \frac{\sigma}{\sigma_0}$; P_0 is a material parameter.

The molecular diffusion of vapour is governed by Fick's law:

$$\mathbf{i}_g^w = -\mathbf{D}_g^w \nabla \omega_g^w = -(\phi \rho_g S_g \tau \mathbf{D}_m^w \mathbf{I} + \rho_g \mathbf{D}'_g) \cdot \nabla \omega_g^w \quad (6.13)$$

where \mathbf{i}_g^w is the non advective mass flux of water in gas, \mathbf{D}_g^w is the dispersion tensor, ω_g^w is the mass fraction of water in gas, τ is the tortuosity and \mathbf{D}'_g is the mechanical dispersion tensor. Usually, a constant dispersion coefficient corresponding to the molecular diffusion of vapour in air is assumed:

$$D_m^w = \tau D \left(\frac{(273.15+T)^n}{P_g} \right) \quad (6.14)$$

where P_g is given in MPa. For τ a value equal to 0.8, for n a value of 2.3 and for D a value of $5.9e-12$ has been adopted. \mathbf{D}'_g can be neglected if air flow is insignificant.

In saturated porous materials, mechanical behaviour is best understood in terms of effective stress $\boldsymbol{\sigma}' = \boldsymbol{\sigma} - P_l \mathbf{m}$, where \mathbf{m}^T is an auxiliary vector [1,1,1,0,0,0]. For unsaturated materials it is necessary to consider two independent stress variables: net stresses ($\boldsymbol{\sigma} - P_l \mathbf{m}$) and capillary suction $s = (P_g - P_l)$. The net stress is the excess of total stress over gas pressure. If full saturation is achieved, net stress becomes effective stress. The mechanical constitutive equation takes the incremental form:

$$d\boldsymbol{\sigma}' = \mathbf{D} d\boldsymbol{\varepsilon} + h ds \quad (6.15)$$

where $\boldsymbol{\sigma}'$ is now used for net stresses, $\boldsymbol{\varepsilon}$ is the strain tensor. \mathbf{D} is the constitutive stiffness matrix, defined by Young's modulus E_i , shear modulus G and Poisson's

ratio v_i through the classical elasticity and h is a constitutive vector relating changes of suction to changes in net stress.

6.1.5 Material parameters

A number of parameters associated with the above equations are material specific parameters which are to be determined by laboratory and in situ experiments. Based on /ZHA 04/, /ZHA 07/, ZHA 08/ and /BOC 08/ the material parameters associated with the constitutive equations implemented in CODE_BRIGHT were determined for Opalinus clay and used in the documented calculations. The values of the parameters are represented in tab. 6.1.

Tab. 6.1 Material parameters determined for Opalinus clay and associated with the constitutive equations

Retention curve equation (6.12)			
P_0	$\sigma_0 [20^\circ\text{C}]$	β	
MPa	N/m	-	
12	0.072	0.3	
Intrinsic Permeability equation (6.9)			
K_{11}	K_{22}	K_{33}	ϕ_0
m^2	m^2	m^2	-
2.00E-20	2.00E-20	6.00E-21	0
Liquid Phase Relative Permeability equation (6.11a)			
A	λ		
-	-		
1	5		
Linear Elasticity equation (6.15)			
E	ν	ϕ_0	ϕ_{\min}
MPa	-	-	-
7000	0.29	0	0

6.2 Numerical simulation

6.2.1 Model geometry and boundary conditions

The 2-dimensional model with its state of plain strain used for numerical simulation is 106 m in height and in length. The BET test gallery is assumed to be perpendicular to the security tunnel and the geometry is supposed to be similar to the Gallery 04 respectively to the Gallery 08 dimensions, which were taken from the MB experiment, /WIE 10/.

In fig. 6.1 it can be seen, that the BET test gallery is located in the centre of the model at about 5.6 m distance to the sensors BET 2 and BET 5. With regard to fig. 4.1 and the presented borehole orientation the used 2-dimensional model takes into account the shortest distance between sensor head and drift contour. The BET test intervals were abstracted and modelled as cylindrical boreholes of 20 mm in diameter without any further instrumentation to keep the calculation effort as low as possible. In order to have the possibility to get anisotropic hydraulic effects at a later stage of numerical simulation two identical boreholes were modelled parallel and perpendicular to bedding plane orientation.

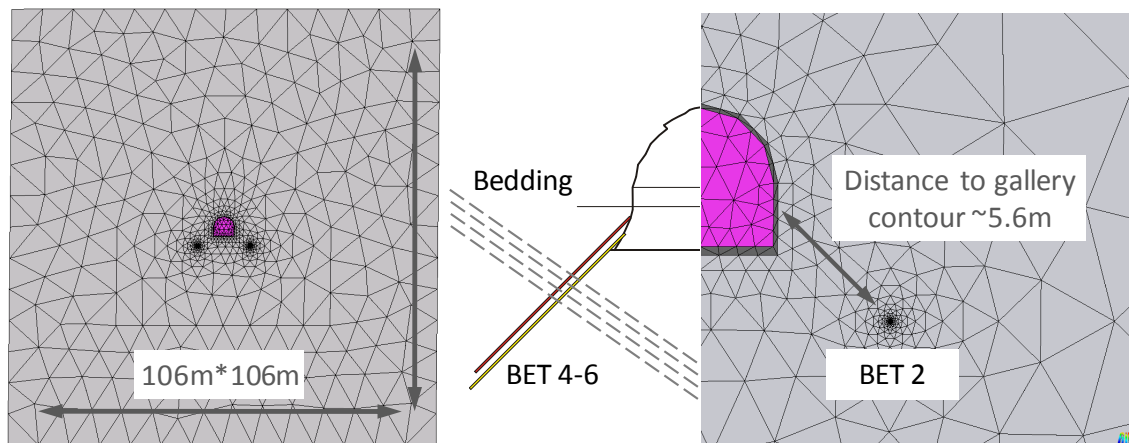


Fig. 6.1 FE model (2D) used for numerical simulation on water and gas injection test at BET test gallery

At Mont Terri the maximum principal stress at laboratory level is in the order of $\sigma_v = 6.5$ MPa, subvertically oriented and its magnitude corresponds to the overburden of 250 m to 300 m. The two subhorizontal principal stresses are roughly aligned with respectively perpendicular to the orientation of the security tunnel. The described

stress state can be considered a best estimate only because stress measurements in clay rich rocks are difficult. The difficulties are the result of the low strength, the high anisotropy and the swelling properties of the Opalinus clay. An extensive discussion of the stress state can be found in /MAR 03/.

According to /VIE 06/ the minor principal stress, which is perpendicular to the orientation of the security tunnel, is assumed to be $\sigma_h = 2.2$ MPa, whereas the intermediate principal stress is parallel oriented and its value is about $\sigma_H = 4.3$ MPa.

Intact Opalinus clay exhibits a very low water permeability, with a mean value of $k = 2.0 \cdot 10^{-20} \text{ m}^2$ for the rock matrix and a much lower value in the direction perpendicular to the bedding planes of $k = 0.6 \cdot 10^{-20} \text{ m}^2$. The very fine pore network is assumed to be fully saturated with an average porosity of 13.7 %, /BOC 08/.

Due to previous numerical experiences in the frame of the Gallery 08 excavation the pore pressure is assumed to be $p_w = 1.5 - 2.0$ MPa at laboratory scale, /WIE 10/.

The existence of a positive pore water pressure around the sensor intervals could not be detected by analysis of the measurement data. For basic numerical investigations on water and gas interaction in claystone rock mass a small area around borehole sensor BET 2 was modelled with 1 m in length and in height. In fig. 6.2 the location of the selected area with respect to the BET test gallery could be seen as well as the relatively fine meshed rock zone (highlighted in dark colour) around the borehole contour of sensor interval BET 2.

The BET 2 sensor interval is located in the centre of the modelled square meter. The claystone rock mass is supposed to be nearly full saturated with a saturation degree of $S_w = 99,9$ %, that is specified by the given boundary parameters for the gas phase at atmospheric pressure $p_{\text{gas}} = 0.1$ MPa and a negative pore pressure value of about $p_w = -0.1$ MPa for the whole model before borehole excavation. The water permeability is supposed to be isotropic with a mean value of $k = 2.0 \cdot 10^{-20} \text{ m}^2$ whereas the mechanical stress state is supposed to be anisotropic, the influence of gravity is neglected.

For comparison with experimental findings two representable nodes within this fine meshed rock zone were selected and the achieved calculation results for node no. 150

at borehole contour zone and node no. 125 in the surrounding rock mass were shown in the following figures.

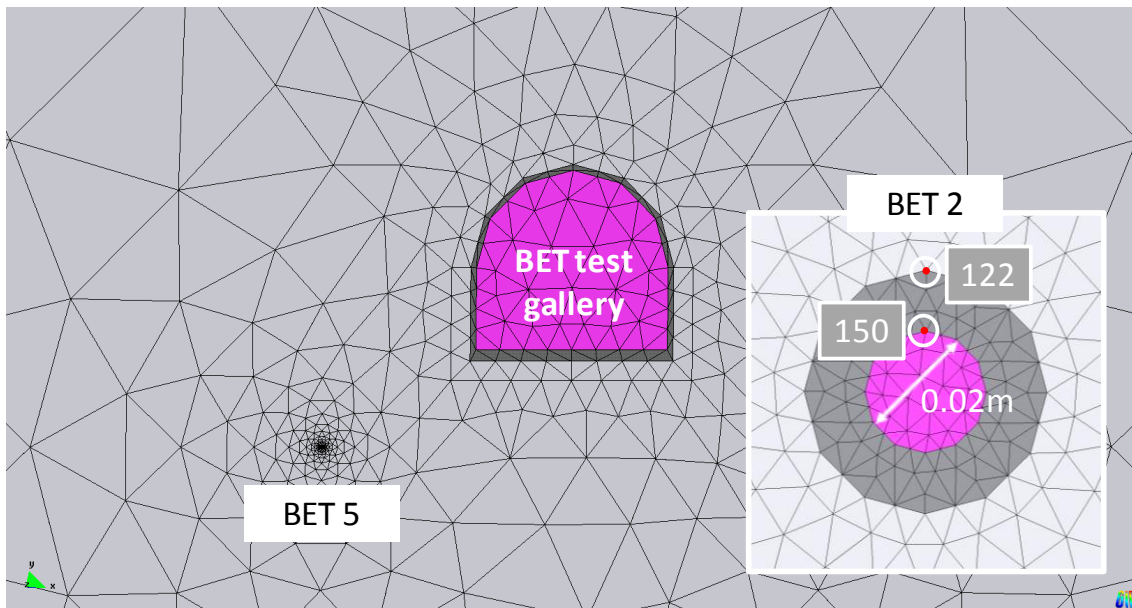


Fig. 6.2 Detailed view of the selected FE model (2D) used for basic numerical investigations of borehole sensor BET 2 on water and gas interaction

6.2.2 Calculation sequence

The numerical simulation work that is presented in the following chapter is separated in two parts:

For basic numerical investigations on water and gas interaction in claystone rock mass the simulation process starts with the excavation of borehole BET 2 on January 25, 2007 followed by a 2 day period of drainage induced by setting the hydraulic boundary condition to a negative pore pressure value of about $p_w = -5.0$ MPa. On January 27, 2007 the sensor has been installed and the water pressure is set to $p_w = 0.1$ MPa and kept constant until the first water injection tests was performed on February 20, 2007. Within this first part of simulation work the whole experimental time from borehole excavation to the second gas injection test on December 15, 2009 has been modelled and selected coupling effects of water and gas phase have been highlighted.

The second part is due to the fact, that the whole simulation process should go along with the realistic time schedule as far as possible, which means that the excavation process of the BET test gallery is simulated within this advanced simulation work as

well as a timeframe of about 2 years for system drainage before BET borehole excavation takes place.

6.3 Analysis and interpretation

Basic numerical investigation

Figure 6.3 shows hydro-mechanical coupled calculation results obtained at the borehole contour zone using a simple constitutive model compared to the observed borehole measurement results for the whole testing time from borehole excavation on January 25, 2007 to the second gas injection test on December 15, 2009.

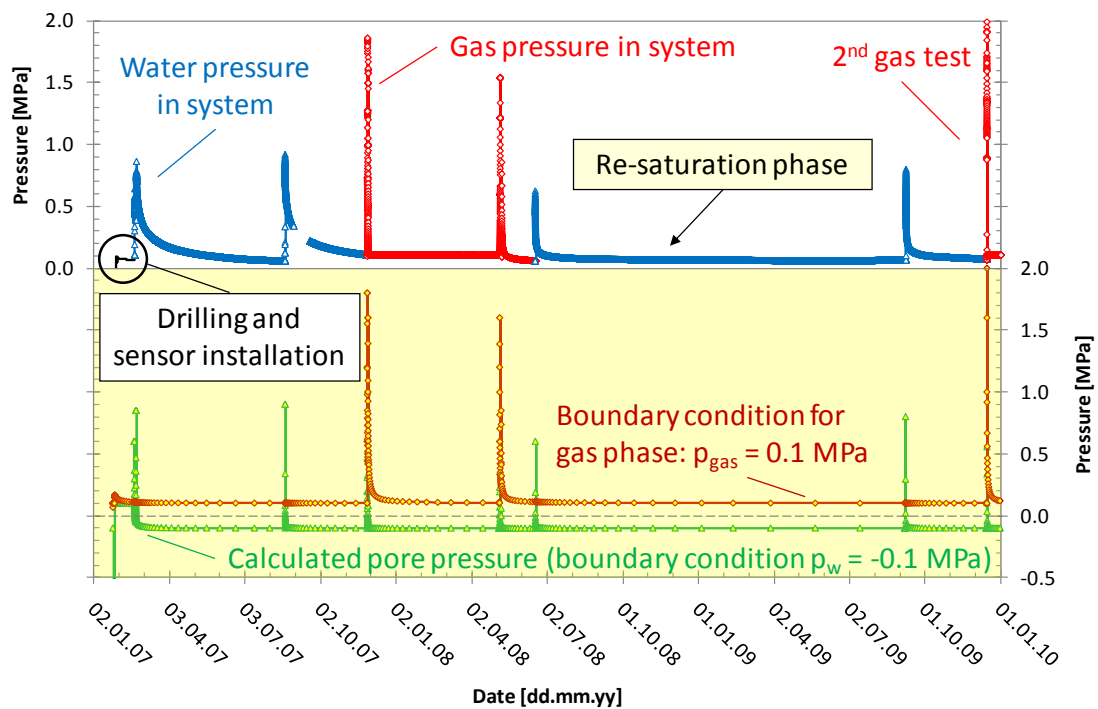


Fig. 6.3 Water pressure and gas pressure values – experimental findings vs. calculation results

The upper part of the diagram shows on the left ordinate the experimental findings on water pressure marked in blue and the values for gas pressure marked in red. In addition the calculation results at borehole contour for gas pressure are marked in brown respectively the results for water pressure are marked in green and shown in the lower part of the diagram on the right ordinate. For additional differentiation the calculation results are highlighted in yellow.

On one hand it is quite obvious to separate the different injection test periods due to the injected medium. On the other hand the adherence to the modelling boundary conditions for gas pressure and water pressure as well as their interaction during the test interval is illustrated by fig. 6.3. Therefore the introduced diagram layout will be used also for further analysis and interpretation of calculation data with respect to experimental findings.

In addition fig. 6.4 shows in the lower part of the diagram on the right ordinate selected calculation results for radial displacements at borehole contour marked in green and the corresponding displacements in the surrounding rock mass marked in brown. The calculation results at the contour zone show the adherence to the modelling boundary conditions whereas the radial displacements in the surrounding rock mass show different reactions to the injection test intervals.

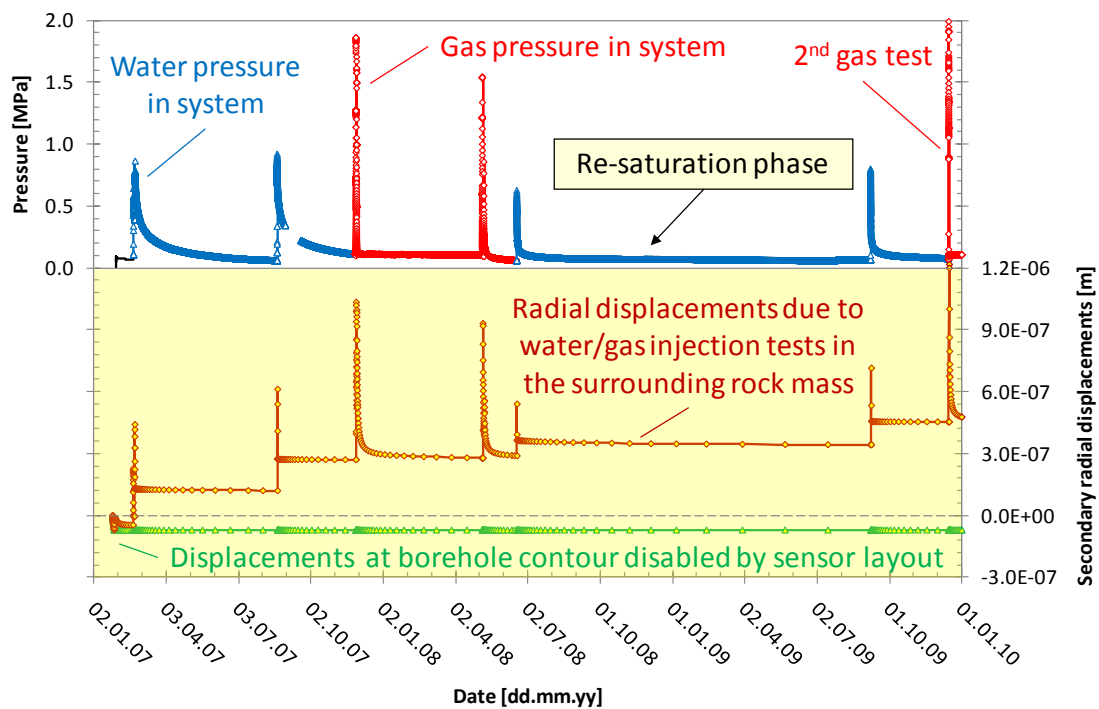


Fig. 6.4 Calculated radial displacements at borehole contour zone and in the surrounding rock mass as a result of basic hydro-mechanical coupled numerical simulation of the BET 2 water and gas injection tests

Due to the borehole excavation process the calculated displacement values show a convergent behaviour. When the sensor is installed and the test interval is filled with water further displacements at the borehole contour zone are disabled.

The increase in water pressure during the first water injection test on February 20, 2007 causes divergent deformation behaviour in the surrounding rock mass. When the injected water pressure is no longer kept constant and the water pressure decreases due to possible dispersion into the pore network, the rock mass converges again. This deformation behaviour could be described by the elastic response of the rock due to stress distribution.

However it has to be highlighted that the deformations have not reached the same level than before the test. There is still a divergent radial deformation part with respect to the initial deformation level remaining. The same effect can be observed during the following water injection test intervals.

Due to the increase in gas pressure the calculation results for the radial deformation in the surrounding rock mass also show a divergent elastic response. In contrast to the test intervals with water the gas injection tests lead to the same deformation level than before the test. A possible explanation could be that the inflow of water into the rock mass due to the increase in water pressure leads to pore water pressure gradients that cause irreversible stress distribution. The observed different levels of radial deformation could be related to this new stress state. Whereas the inflow of gas into the rock mass due to the increase on gas pressure replaces the water in the rock matrix for the time the gas pressure is kept constant during the test. As a consequence the replacement of water must lead to de-saturation.

Figure 6.5 shows in the lower part of the diagram on the right ordinate selected calculation results for the saturation degree at borehole contour marked in green and the corresponding values in the surrounding rock mass marked in brown.

As expected the gas injection leads to de-saturation of the contour zone whereas a re-saturation process is shown that is due to the water pressure built-up during water injection tests.

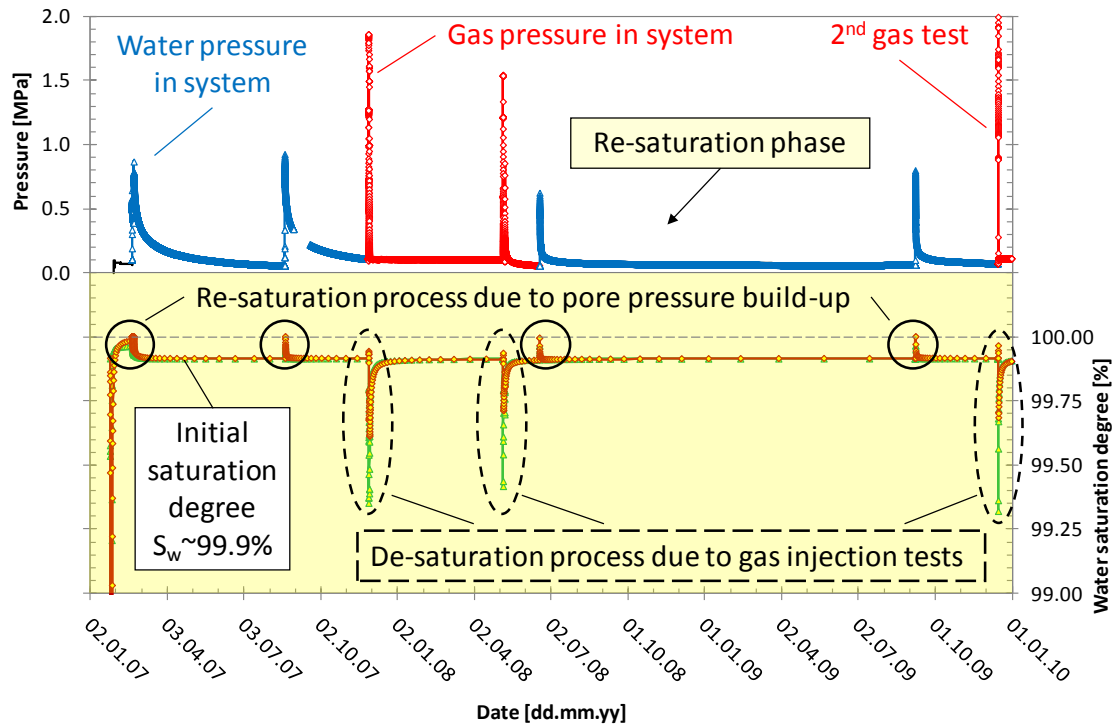


Fig. 6.5 Calculated water saturation degree at borehole contour zone and in the surrounding rock mass as a result of basic hydro-mechanical coupled numerical simulation of the BET 2 water and gas injection test intervals

Moreover the increase in water pressure as a reaction to the simulated gas pressure increase is one of the noticeable effects that need to be investigated in more detail. Figure 6.6 therefore shows calculation results of the first gas injection test sequence from November 28, 2007. The upper part of the diagram shows on the left ordinate the calculated values for water pressure marked in blue and the values for gas pressure marked in red, allocated to the nodes at borehole contour zone and in the surrounding rock mass. In addition the calculated saturation degree in the surrounding rock mass is marked in brown respectively the results at the contour zone are marked in green and shown in the lower part of the diagram on the right ordinate. For additional differentiation the time period when the gas pressure has been controlled is highlighted in yellow.

During the gas injection phase the gas flow into the fine pore structure network of the claystone rock mass is expected to replace the existing mass of water. The water flow is restricted to the very low water permeability with a mean value of $k = 2.0 \cdot 10^{-20} \text{ m}^2$. The limited water flow process leads to an increase in water pressure at the contour zone that is followed by pore water dispersion into the surrounding rock mass. The marginal increase in saturation could be explained by this dispersion process.

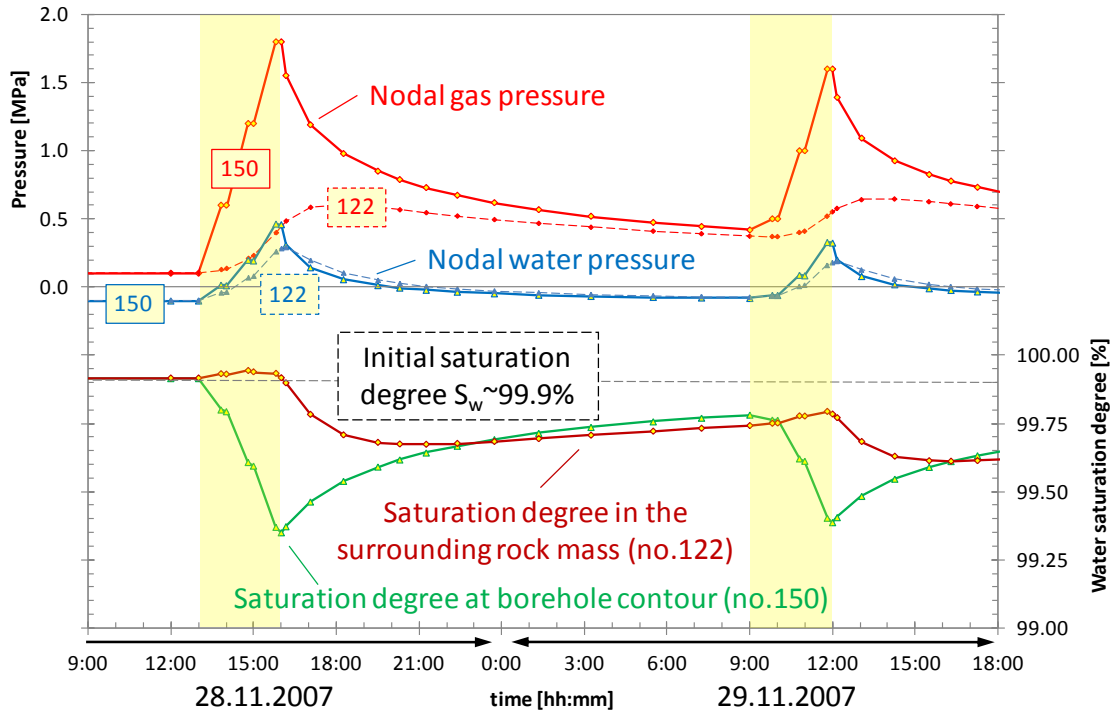


Fig. 6.6 Calculated water and gas pressure in comparison with saturation degree values as a result of basic hydro-mechanical coupled numerical simulation of the first BET 2 gas injection test interval

Simultaneously, the gas flow into the contour zone due to the increase in gas pressure leads to de-saturation. Although the radial deformation of the contour zone is disabled by sensor layout the gas density increases.

When the gas injection pressure is no longer controlled by the testing design the pore water dispersion leads to a degradation of pore water pressures. Due to the boundary conditions the gas density at the borehole contour is reduced by diffusion (degradation of concentration gradients) with time. The saturation degree at borehole contour zone increases again whereas the gas flow into the surrounding rock mass decreases the water saturation degree.

Advanced simulation work

The whole simulation process should go along with the realistic time schedule as far as possible, which means that after the excavation process of the BET test gallery is simulated within advanced simulation work the whole system underlies a simulation time of about 2 years for drainage (from end of November 04 to end of January 07).

The excavation process of the BET test gallery causes stress distributions that lead to compressive deformations of the rock matrix near the drift wall. While using an elastic hydro-mechanical coupled approach this compressive deformation is followed by an increase in pore water pressure exceeding the hydrostatic value up to $p_w = 3.2$ MPa.

In the following this high pressure gradient is reduced by pore water dispersion. The dispersions process is restricted to the water permeability of the rock mass. Due to the capabilities of the adopted simplified approach without taking into account any damaging process the development of an excavation damaged zone (EDZ) at the gallery contour is simulated via a time-dependent de-saturation process of the surrounding rock mass induced by setting the hydraulic boundary condition to a negative pore pressure of about $p_w = -5.0$ MPa. Consequently the pore pressure field will vary with time.

Though the existence of a positive pore water pressure around the sensor intervals could not be detected by analysis of the measurement data it is obvious that the advanced simulation work should reflect the observed experimental findings during the simulation process. Therefore the calculation results including the gallery excavation as well as the borehole excavation and the first water pressure testing intervals were taken for validation of the physical model.

When taking into account a simulation time of about 2 years for drainage the level of pore water decrease near to the gallery contour is restricted to the water permeability value of the rock matrix. Therefore fig. 6.7 shows the sensitive dissipation behaviour of the rock matrix at the borehole contour zone when the value of water permeability is increased just in one order of magnitude from $k = 2.0 \cdot 10^{-20} \text{ m}^2$ to $k = 2.0 \cdot 10^{-19} \text{ m}^2$.

Whilst using a value for water permeability of $k = 2.0 \cdot 10^{-20} \text{ m}^2$ the dissipation process is underestimated, whereas the value of $k = 2.0 \cdot 10^{-19} \text{ m}^2$ overestimates the water flow and leads to de-saturation of the rock mass after 1.5 years of simulation time. The curve-

fitting process leads to a value of $k = 1.1 \cdot 10^{-19} \text{ m}^2$ for water permeability that represents the observed hydraulic behaviour at its best. After 2 years simulation time of system drainage the atmospheric pressure front nearly reaches the area where the BET boreholes are located. When the water injection test is finished and the water pressure is no longer kept constant the water pressure decreases down to the observed level of $p_w = 0.1 \text{ MPa}$ or even down to capillary pressure values, which are not measurable with the existing equipment.

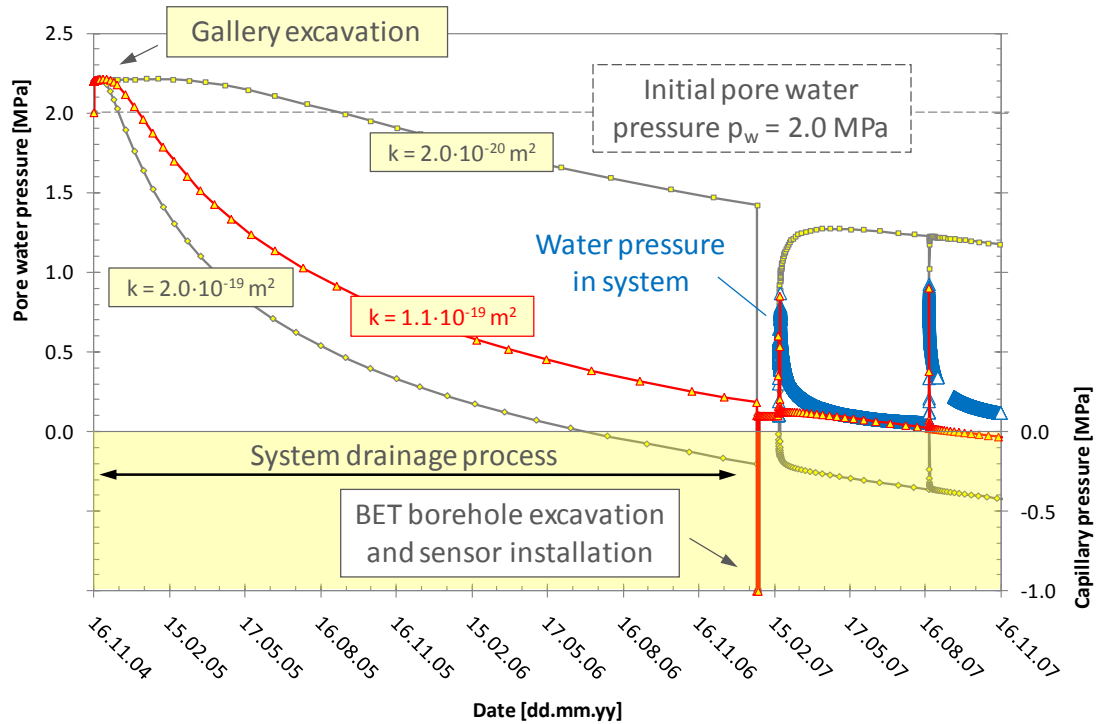


Fig. 6.7 Calculated water pressure at borehole contour zone with different water permeability values as a result of advanced hydro-mechanical coupled numerical simulation including the gallery excavation as well as the borehole excavation and the first water pressure testing intervals

With respect to the modified value of water permeability of the rock matrix fig. 6.8 shows calculation results on pore pressure dispersion as a result of hydro-mechanical coupled numerical simulation for November 17, 2004 1 day after the gallery excavation process at the BET test location and for January 25, 2007 after 2 years of system drainage before the BET boreholes were excavated.

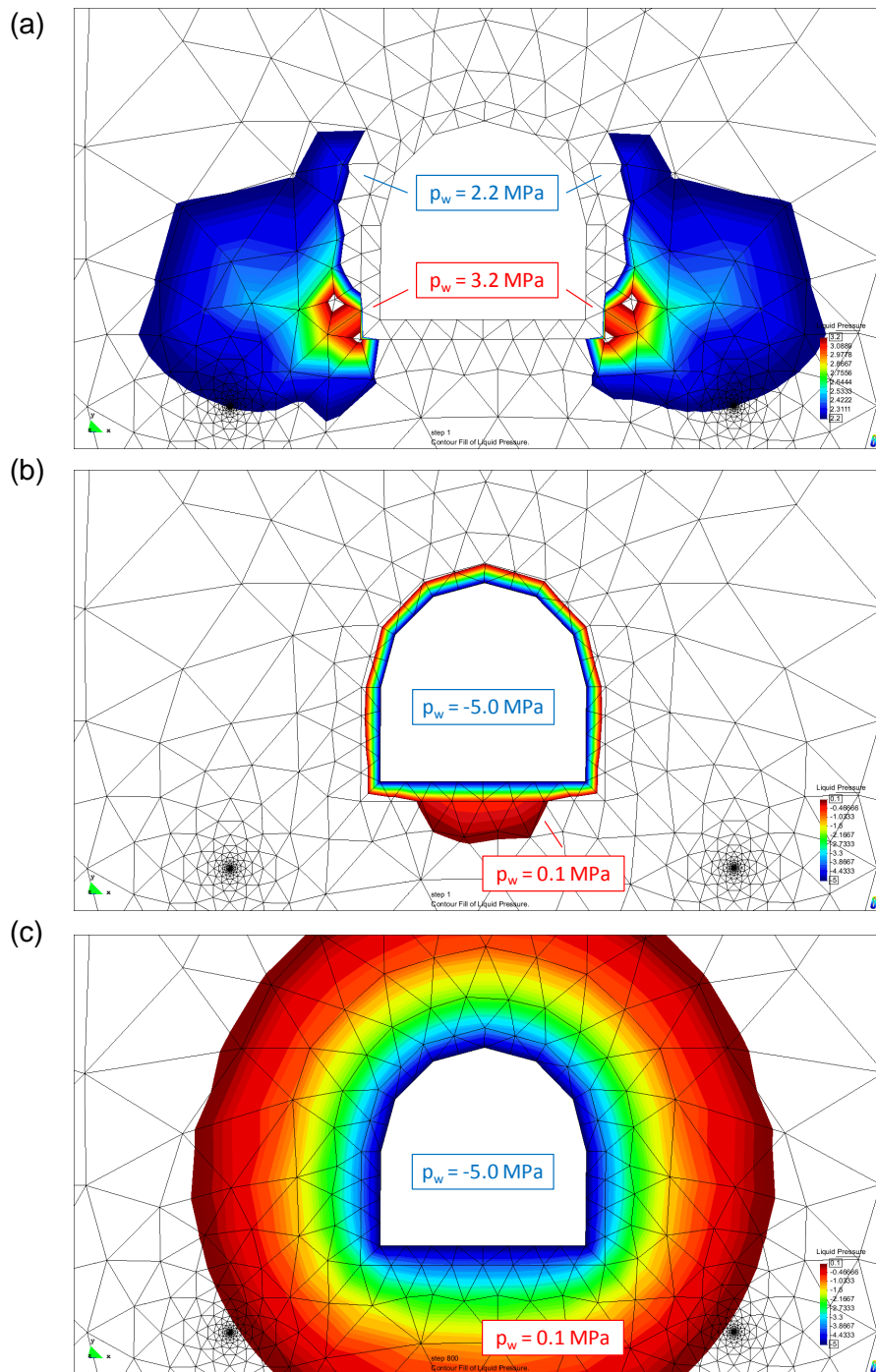


Fig. 6.8 Calculated pore water pressure as a result of advanced hydro-mechanical coupled numerical simulation of gallery excavation

1 day after on November 17, 2004

(a) Pore water pressure $p_w > p_{w0}$

(b) Negative pore water pressure $p_w < p_{atmos}$

2 years of system drainage before borehole BET excavation on January 25, 2007

(c) Negative pore water pressure $p_w < p_{atmos}$

Due to numerical stability problems it was not possible to simulate the gas pressure evolution in the rock mass during the gas pressure injection test within the advanced simulation work.

The following discussion in chapter 7.3 therefore deals with the identified deficits of the physical modelling approach used for numerical simulation of water and gas interaction with respect to calculation effort and confidence of the results.

7 Discussion

7.1 In-situ investigations

Pore pressure and saturation

Except for borehole BET 6 with an initial pore pressure of 0.17 MPa, all BET boreholes showed pore pressures at atmospheric or below prior to the first injection tests in February 2007. A pore pressure below atmospheric means suction and occurs when the rock is not fully saturated. Since the BET experiments aimed at the investigation of gas transport in undisturbed rock a significant undersaturation would have impaired the relevance of the results. The advanced model calculations showed that with the observed pore pressures the rock is still fully saturated in a technical sense (saturation above 99 %). In order to make sure that the results are relevant, the additional boreholes BMB 3 and BMB 4 were used for testing. In these boreholes, pore pressures between 0.5 MPa and 1 MPa had been measured.

After the first and second gas injection campaigns, the pressure remained at elevated values in the boreholes BET 5 and BET 6 as a consequence of the limited pore space available for gas dissipation.

Permeability to water

The permeability values after the first water injection campaigns in February and August 2007 yielded rather homogeneous values in the range of 10^{-19} m^2 , with a somewhat lower value at BET 6 and a high value for BET 1 which is, however, not reliable due to the fact that this test interval could not be re-saturated. The water injection tests in June 2008 were performed shortly after gas injection testing when gas was still present in the surrounding rock. Consequently, the values for the water permeability show greater variations and are less relevant, the measurement at BET 6 was not evaluable at all. After re-saturation of the test intervals and the 18 months rest period, the permeability values show less scatter and are closer to the original values.

The water injection tests performed at BMB 3 and BMB 4 yielded values of $4 \cdot 10^{-19} \text{ m}^2$ and $8 \cdot 10^{-21} \text{ m}^2$, respectively.

Gas entry pressure

The in-situ investigations showed initial gas entry pressures for most of the boreholes in the range around 1.8 MPa to 2.5 MPa. In the BET boreholes, a dependence on the geometry is visible: The initial gas entry pressures in the test intervals increase with borehole depth, and they are generally somewhat lower in the boreholes drilled parallel to the bedding than normal to the bedding. In the deepest boreholes, gas entry pressure is higher than 2.5 MPa (3.2 MPa parallel to bedding, > 5 MPa normal to bedding). These results comply with the findings of the HG-C project /JOC 08/.

The deep boreholes BMB 3 and BMB 4, however, show gas entry pressures of about 2 MPa. It is therefore assumed that a gas entry pressure around 2 MPa is the “normal” case, while limited regions with higher gas entry pressure may exist, depending on rock composition and homogeneity, stress state, and saturation.

Repeating the gas injection after one day (BET 2, BET 5) led to considerably lower entry pressures, which is not surprising since pathways had already been created and gas was still in the system.

The repetition of gas injection after 6 months without an interim re-saturation (BET 2, BET 5) still showed a significant reduction of gas entry pressure in comparison to the original values, although a partial recovery of entry pressure could be observed. Considering the reduction of gas entry pressure as a consequence of gas-pressure induced damage which leads to the formation of additional pore space, this result is in agreement with the laboratory tests on small samples which showed higher gas permeabilities when injection tests were repeated. It also agrees well with the observations on the large samples which showed a much lower gas entry pressure for the damaged sample in comparison to the intact one. The gas entry pressure of the re-saturated intact sample of 3.8 MPa is somewhat higher than most of the in-situ values, which may be a consequence of the test geometry and stress conditions.

After re-saturation of the test intervals and a rest period of 18 months, the gas entry pressures increased again by 0.5 MPa to 1 MPa and nearly reached the original values (BET 2 and BET 5) or was even higher (BET 4). This result shows that all gas had left the system in the meantime and that pathways created by the earlier gas injection cycles were widely re-sealed.

The anomalous behaviour of BET 1 is associated to the fact that the return tube, and, during the injection phase in December 2009, probably also the injection tube, was blocked.

Apparent gas permeability

During the gas injection tests, several pressure steps were applied to the different test intervals. After gas entry, the gas pressure load resulted in quasistatic gas flow into the formation which was evaluated in terms of an apparent gas permeability using the radial formulation of the Darcy equation.

Depending on the injection pressure apparent gas permeabilities between 10^{-19} m^2 and 10^{-15} m^2 were obtained. A clear dependence between injection pressure and permeability was found for the BET boreholes. Especially during the last gas injection campaign it was ascertained that the apparent gas permeability steadily increased and decreased with increasing and decreasing injection pressure, which confirms the mechanism of dilatant widening or closing of pathways which was already assumed during the HG-C investigation /JOC 08/ and is in agreement with the laboratory results.

BET 1 exhibited an anomalous behaviour. During the last gas injection campaign, no gas flow was observed until, at an injection pressure of 3 MPa, a gas-frac occurred. Considering the fact that earlier injection tests had confirmed that the rock around this interval was not saturated and the gas entry pressure was much lower, it is suspected that the injection tube was blocked during the test and cleared only at the high pressure of 3 MPa, which then led to the frac.

The gas injection tests at BMB 3 and BMB 4 exhibit a much less pronounced dependence of apparent gas permeability on the injection pressure. Reasons for this may be the different stress and pore pressure conditions or differences in mineral composition.

Recompaction

The observations of gas entry pressure and apparent gas permeability before and after re-saturation of the test intervals and an 18-months rest period show the great potential of self-sealing of the clay rock. Damage itself is, in the case of a moderate gas pressure increase, limited to the dilatant widening of pathways, which reduce again as

soon as the gas pressure decreases. When the gas has left the system, the original gas entry pressure and permeability to water are nearly restored.

7.2 Laboratory results

Investigations on small samples

First experiments under isostatic load showed that gas injection pressure has a clear influence on gas permeability. The permeability evolution below loading pressure hints to an opening and closing of pathways. Repetition of measurements showed increased permeabilities with respect to original values, which shows that pathways were not completely re-sealed within the experiment time. This is in agreement with the in-situ observations during the first injection campaigns, before re-saturation and 18 months rest period.

Investigations under triaxial load showed first that an axial load exceeding the radial load led to decrease in gas permeability, which can be explained by a mechanical sealing of existing (radial) pathways. The following tests with varying mechanical loads and injection pressures confirmed the principle behaviour of the gas permeability increasing with injection pressure. This is especially evident at pressures exceeding 2 MPa, which coincides with the in-situ gas entry pressure.

Experiments with an increased temperature up to 90 °C and a constant injection pressure far below the constant isostatic load showed a water release from the sample starting at a temperature of about 50 °C. Gas permeability was increasing with time, which can be explained by expulsion of water causing an increase in available pathways for gas. The water release stopped when the temperature was reduced again.

Large samples

Investigations on large core samples were performed in order to check the transferability of the results and exclude scaling effects.

Investigations using the damaged sample showed a clear influence of the fracture on the behaviour, so that even low gas injection pressures resulted in relatively high flow rates. Again, an increase of gas permeability with injection pressure was visible. A later

permeability reduction can probably be explained by swelling effects caused by the moisture contained in the nitrogen used for the measurement.

In order to investigate the self-sealing behaviour, Pearson water was injected into the sample. The subsequent measurements of permeability to water also showed a permeability increase with injection pressure. Water permeability values were altogether lower than the gas permeabilities determined earlier. After the water injection tests a measurement of the gas entry pressure yielded a value of 0.4 MPa. The gas permeabilities measured after gas break-through were significantly lower than before re-saturation of the sample. Even further increase of injection pressure did not restore the original gas permeability value. This is explained by swelling of the sample and reduction of pathways for gas by water and confirms the self-sealing capacity of the clay rock. It complies with the observations during the in-situ testing before and after test interval re-saturation and rest period.

For the intact sample, the initial gas permeability was by a factor of 2.5 lower than for the damaged one. It also increased with injection pressure. Repeating the injection tests resulted in nearly identical permeabilities, so that a permanent damage by gas injection can be excluded.

Similarly to the other large sample Pearson water was then injected. For a period of 57 days the sample took up water, but no water release could be detected at the outer surface. A subsequent gas injection yielded a gas entry pressure of 3.8 MPa. A reduction of injection pressure after gas break-through again led to a reduction of gas permeability.

Both the damaged and the intact sample showed a comparable behaviour with respect to the gas injection pressure/permeability relation. It is remarkable that even the damaged and restored sample showed a dilatant behaviour with no further permanent damaging. Differences exist only regarding the order of magnitude of permeability to gas and water and the gas entry pressure after re-saturation.

„Healing“ of the failed bedding plane after the injection of Pearson water was observed when the damaged sample was dismantled at the end of the test.

In all tests permeability changes, increasing or decreasing, took place continuously, which confirms that the mechanism of permeability change is dilatant widening or closing of pathways.

Fracture visualisation

Fracture visualisation by scanning of individual layers showed fine fracture structures, which can open or close by variation of injection pressure. Thus, the hydraulic behaviour of the clay rock can be explained plausibly and coherently.

7.3 Numerical investigations

Basic numerical investigation

Regarding the tight coupling between fluid flow processes and mechanical deformation in argillaceous rock mass a simplified approach has been used for basic and advanced numerical investigations of water and gas interaction with respect to measurement results at BET test gallery at Mont Terri URL. Though the existence of a positive pore water pressure around the sensor intervals could not be detected by analysis of the measurement data a small area around borehole sensor BET 2 was modelled and has been used for basic numerical investigations. The claystone rock mass was supposed to be nearly full saturated with a saturation degree of $S_w = 99.9\%$, that was specified by the given boundary conditions for the gas phase at atmospheric pressure $p_{\text{gas}} = 0.1 \text{ MPa}$ and a negative pore pressure value of about $p_w = -0.1 \text{ MPa}$ for the whole model before borehole excavation. The water permeability was supposed to be isotropic with a mean value of $k = 2.0 \cdot 10^{-20} \text{ m}^2$ whereas the mechanical stress state was supposed to be anisotropic. The influence of gravity was neglected.

Due to the borehole excavation process the calculated displacement values showed a convergent behaviour. When the sensor was installed and the test interval was filled with water further displacements at the borehole contour zone were disabled. The increase in water pressure during the first water injection test caused divergent deformation behaviour in the surrounding rock mass. When the injected water pressure was no longer kept constant and the water pressure decreased due to possible dispersion into the pore network, the rock mass converged again. This deformation behaviour could be described by the elastic response of the rock due to stress distribution. The deformations, however, have not reached the same level than before

the injection test. There is still a divergent radial deformation part with respect to the initial deformation level remaining. The same effect has been observed during the following water injection tests.

Due to the increase in gas pressure the calculation results for radial deformation in the surrounding rock mass also show a divergent elastic response. In contrast to the tests with water the gas injection tests lead to the same deformation level as before the test.

In principle, the different level of radial deformation in the surrounding rock mass achieved during the modelling process of gas and water injection tests could be described by the different compressive behaviour of the injection media. The injected mass of water dissipates into the pore structure and leads to irreversible stress distributions, whereas the injected mass of gas leads to an increase in gas density during the injection phase and decreases afterwards without an irreversible effect on stress distribution.

During the gas injection phase the gas flow into the fine pore structure network of the claystone rock mass is expected to replace the existing mass of water. The water flow is restricted to the very low water permeability with a mean value of $k = 2.0 \cdot 10^{-20} \text{ m}^2$. The limited water flow process leads to an increase in water pressure at the contour zone that is followed by pore water dissipation into the surrounding rock mass. Simultaneously, the gas flow into the contour zone due to the increase in gas pressure leads to de-saturation. Although the radial deformation of the contour zone is disabled by sensor layout the gas density increases. When the gas injection pressure is no longer controlled by the testing design the pore water dissipation leads to a degradation of pore water pressures. Due to the boundary conditions the gas density is reduced by diffusion (degradation of concentration gradients) with time. The saturation degree at borehole contour zone increases again whereas the gas flow into the surrounding rock mass decreases the water saturation degree.

Advanced simulation work

For advanced modelling the excavation process of the BET test gallery was simulated including a simulation time of about 2 years for system drainage without taking into account any damaging process. With regard to the experimental findings the performed curve-fitting process leads to a value of $k = 1.1 \cdot 10^{-19} \text{ m}^2$ for water permeability that represents the observed hydraulic behaviour of the claystone rock mass at its best.

In contrast to the basic numerical investigations the pore structure of the rock was supposed to be fully saturated and an initial pore water pressure of $p_w = 2.0$ MPa was assumed at laboratory scale. Although basic investigations have shown the possibility to model the evolution of positive pore pressure values and the de-saturation process due to a parallel gas pressure increase within the same zone, it was not possible to simulate the gas pressure evolution in the rock mass during the gas pressure injection test within the advanced simulation work.

Deficits in physical modelling and numerical simulation

The advanced calculations disclose some deficits with the implementation of the existing constitutive laws leading to unexpected numerical problems. Further numerical investigations in this respect should focus on:

- Influence of hydraulic boundary conditions for water and gas phase, when the pore structure of the observed rock mass is assumed to be fully saturated exhibiting a hydrostatic pore water pressure gradient
- Level of de-saturation due to increase in gas density
- Limiting values for increasing gas density

Regarding the objectives of this project the observed effect of increasing gas flow due to gas pressure induced dilatant opening of the pore structure network could not be represented by the existing physical modelling approach. Therefore the development of advanced computer codes for numerical simulation of hydro-mechanical coupled processes with respect to water and gas interaction in claystone rock mass demands improved and specialized constitutive laws. This demand requires additional knowledge about mechanisms and parameters to understand, describe, and model the rock mass behaviour in a sufficiently realistic way. Specifically, a constitutive law coupling pore pressure to reversible deformation (dilatant opening/closing of pore space) has to be developed and implemented.

With respect to today's demand for coupling of THM(C)-processes, validating the forecasting tools which are applied for physical modelling and numerical simulation remains a demanding task.

7.4 Comparison to rock salt behaviour

Comparably to the investigations presented here, the Institut für Gebirgsmechanik (IfG) performed gas injection tests at pressures in the range of the minimum rock stress in rock salt, complemented by laboratory testing on salt samples /POP 10/. Similar results were obtained: At a pressure close to the minimum stress the gas flow rate increased significantly, limiting further pressure increase, without leading to a gas-frac. A gas-frac can only occur when the gas production rate is so high that the increased permeability and thus the transport capacity of the rock are not sufficient to avoid further pressure increase. Considering that in a high-level waste repository gas is produced mainly by corrosion, it seems unlikely that this could be the case, both in salt or in clay host rock formations.

In addition, a natural gas-frac that occurred at the Merkers salt mine in 1989 was investigated with respect to the self-sealing capacity of rock salt /POP 08/. Within 18 years after the incident a partial recovery of the salt barrier and partial healing of fractures could be confirmed.

8 Conclusions

In the frame of the BET project, the issue of gas transport in water-saturated clay rock was investigated using a combined approach involving in-situ and laboratory testing as well as numerical modelling. This approach proved profitable, because

- In-situ and laboratory experiments gave complementing information and confirmed the respective results.
- Numerical modelling gave explanations for unexpected behaviour and confirmation of expected one.

All experimental results show that the most relevant gas transport mechanism will be dilatancy controlled gas flow, meaning the dilatant opening and closing of pathways with very limited damaging of the rock. The gas permeability will rise and fall with gas pressure, more or less continuously. The gas permeability values seem high enough for releasing gas pressure as it occurs.

The in-situ tests also showed that after a limited amount of re-saturation time (18 months in the experiment) after gas injection, the original hydraulic behaviour of the rock is nearly restored. The laboratory tests showed that even highly damaged samples with pronounced failure planes will, at least partially, heal in the course of re-saturation over 57 days.

Pneumatic fracturing is in principle possible, but will occur only under very special circumstances that involve applying a high pressure peak suddenly. The laboratory results with damaged samples suggest that pneumatic fractures will not cause irreversible damage.

The numerical simulations were helpful for understanding the situation in the field tests. The employed models, however, lack a formulation to simulate the dilatant opening and closing of pore space. Moreover, deficits were found in the existing implementation of constitutive laws. Further development work is definitely needed in this respect in order to be able to reliably model gas transport in the saturated clay rock. This work will have to include

- Development and implementation of a constitutive law coupling pore pressure to reversible deformation (dilatant opening/closing of pore space),

- Calibration and validation of such a constitutive law,
- Performing realistic predictions of gas pressure and transport in a clay host rock repository.

The BET project has provided useful data for these tasks.

References

- /ABR 04/ Abramoff, M.D., Magelhaes, P.J., Ram, S.J. (2004): "Image Processing with ImageJ".- Biophotonics International, volume 11, issue 7, pp. 36-42.
- /AKE 02/ AkEnd (2002): Auswahlverfahren für Endlagerstandorte. – Empfehlungen des AkEnd - Arbeitskreis Auswahlverfahren Endlagerstandorte, Köln Dezember 2002.
- /BMU 09/ BMU (2009): Safety Requirements Governing the Final Disposal of Heat-Generating Radioactive Waste.- Bundesministerium für Umwelt, Naturschutz und Reaktorsicherheit (BMU). Berlin, July 2009 (Source: <http://www.bmu.de>).
- /BOC 08/ Bock, H. (2008): RA Experiment – Updated Review of the Opalinus Clay at the Mont Terri URL based on Laboratory and Field testing. 2008, TR 2008-04.
- /JOC 08/ Jockwer, N., Wieczorek, K. (2008): Gas Migration in the Opalinus Clay as a Function of the Gas Injection Pressure - HG-C Project. Final Report, GRS-249, Köln.
- /MAR 03/ Martin, C.D., Lanyon, G.W., Blümling, P. (2003): Measurement of in-situ stress in weak rocks at Mont Terri Rock Lab. International Journal of Rock Mechanics and Mining Sciences, 40, p.1077 – 1088.
- /OLI 96/ Olivella, S., Gens, A., Carrera, J., Alonso, E.E. (1996): Numerical Formulation for a Simulator (CODE_BRIGTH) for the Coupled Analysis of Saline Media. Engineering Computations, 1996, Vol. 13, No 7, pp 87-112.
- /POP 08/ Popp, T., W: Minkley (2008): Integrity of a salt barrier during gas pressure build-up in a radioactive waste repository – Implications from laboratory investigations and field studies – REPOSAFE 2007, Radioactive Waste Disposal in Geological Formations, International Conference. Braunschweig, November 6 – 9, 2007. Proceedings.

- /POP 10/ Popp, T., W: Minkley (2010): Salt barrier integrity during gas pressure build-up in a radioactive waste repository – Implications from lab and field investigations. 44thUS Rock Mechanics Symposium and 5th U.S.-Canada Rock Mechanics Symposium, Salt Lake City, UT, June 27–30, 2010. Proceedings.
- /RAS 09/ Rasband, W.S. (2009): Image, J. U. S. National Institutes of Health, Bethesda, Maryland, USA, <http://rsb.info.nih.gov/ij/>, 1997-2009.
- /RUE 04/ Rübél, A.; Nosek, U.; Müller-Lyda, I.; Kröhn, K.-P.; Storck, R. (2004): Konzeptioneller Umgang mit Gasen im Endlager.- GRS-205, Köln.
- /RUE 05/ Rübél, A., Buhmann, D., Noseck, U. (2005): Anwendung sicherheitsanalytischer Instrumentarien für Endlager in Salz- und Tonformationen. Unterschiede und Gemeinsamkeiten. – Vortrag anlässlich des Workshops GEIST, Peine, 19. und 20.01.2005.
- /THU 99/ Thury, M., Bossart, P. (1999): Mont Terri Rock Laboratory – Results of the Hydrogeological, Geochemical and Geotechnical Experiments Performed in 1996 and 1997, Landeshydrologie und –geologie, Geologische Berichte Nr. 23.
- /UPC 02/ UPC (2002): A 3-D program for thermo-hydro-mechanical analysis in geological media.
- /VIE 06/ Vietor, T., Blümling, P., Armand, G. (2006): Failure mechanisms of the Opalinus Clay around underground excavations. EUROCK 2006 ISRM regional symposium on multiphysics coupling and long-term behaviour in rock mechanics, May 2006, Liège, Belgium.
- /WIE 10/ Wieczorek, K., Czaikowski, O. (2010): Hydraulic measurements and interpretative modelling in the frame of the Gallery 08 excavation at URL Mont Terri. Technical Report, *in preparation*.
- ZHA 02/ Zhang, C.-L.; Dittrich, J.; Müller, J.; Rothfuchs, T. (2002): Experimental Study of the Hydromechanical Behaviour of the Callovo-Oxfordian Argillites. Part of the MODEX-REP Project. – GRS-187.

- /ZHA 04/ Zhang, C.-L., Rothfuchs, T., Moog, H., Dittrich, J., Müller, J. (2004): Thermo-Hydro-Mechanical and Geochemical Behaviour of the Callovo-Oxfordian Argillite and the Opalinus Clay.- Final Report, GRS-202, Köln.
- /ZHA 07/ Zhang, C.-L., Rothfuchs, T., Jockwer, N., Wieczorek, K., Dittrich, J., Müller, J., Hartwig, L., Komischke, M. (2007): Thermal Effects on the Opalinus Clay – A Joint Heating Experiment of ANDRA and GRS at the Mont Terri URL (HE-D Project). March 2007, GRS-224.
- /ZHA 08/ Zhang, C.-L., Rothfuchs, T., Dittrich, J., Müller, J. (2008): Investigations on Self-sealing of Indurated Clay. March 2008, GRS-230.

List of figures

Fig. 3.1	Mont Terri motorway tunnel and location of the Mont Terri Rock Laboratory (left centre of the picture)	5
Fig. 3.2	Geological profile along the motorway tunnel showing the location of the Mont Terri Rock Laboratory	6
Fig. 3.3	View of the Mont Terri Rock Laboratory showing the various tunnels with the year of their excavation and the BET experimental sites.....	7
Fig. 3.4	Plan view showing the Mont Terri Rock Laboratory geology	7
Fig. 4.1	Boreholes at the BET test site.....	9
Fig. 4.2	Drilling of test boreholes	10
Fig. 4.3	Minipiezometer installed in the test boreholes.....	11
Fig. 4.4	Transducer rack: BET 1-3 (left) und BET 4-6 (right).....	11
Fig. 4.5	Principle layout of the Data Acquisition System (DAS).....	12
Fig. 4.6	Boreholes BMB 1 – BMB 4 drilled from the HE-B Niche.....	13
Fig. 4.7	Boreholes BMB 1 – BMB 4 drilled from the HE-B Niche.....	14
Fig. 4.8	Borehole collars of BMB 1 – BMB 4 and transducer racks (left)	14
Fig. 4.9	Preparation of the small core samples	19
Fig. 4.10	Preparation of a large core sample	21
Fig. 4.11	Symbolic sample cross section with denotation of variables for permeability calculation.....	23
Fig. 5.1	Pressure evolution in the BET boreholes before the first gas injection tests.....	25
Fig. 5.2	Pressure evolution in the BMB boreholes before the gas injection tests.....	26
Fig. 5.3	Gas injection BET 2 in November 2007: Gas injection pressure and gas tank mass	27
Fig. 5.4	Gas injection BET 5 in November 28, 2007: Gas injection pressure and gas tank mass.....	28
Fig. 5.5	Gas injection BET 2 in May 2008: Gas injection pressure and gas tank mass	29

Fig. 5.6	Gas injection BET 1 in May 2008: Gas injection pressure and gas tank mass	30
Fig. 5.7	Gas injection BET 5 in December 2009: Gas injection pressure and gas tank mass	32
Fig. 5.8	Gas injection BET 3 in December 2009: Gas injection pressure and gas tank mass	33
Fig. 5.9	Gas injection BET 1 in December 2009: Gas injection pressure and gas tank mass	33
Fig. 5.10	Gas injection BMB 3 in December 2009: Gas injection pressure and gas tank mass	34
Fig. 5.11	Test history of sample F: Permeability and injection pressure.....	40
Fig. 5.12	Test history of sample G: Permeability and injection pressure	40
Fig. 5.13	Test history of sample 2: Permeability and injection pressure.....	41
Fig. 5.14	Test history of sample 2: Permeability and water release at elevated temperature.....	42
Fig. 5.15	Test history of sample 2: Permeability and water release at elevated temperature.....	43
Fig. 5.16	Comparison of the gas permeabilities before saturation and after gas break-through and the water permeability (damaged sample 2L)	44
Fig. 5.17	Evolution of gas permeability with time after gas break-through at different gas injection pressures (sample 2L).....	45
Fig. 5.18	Evolution of gas permeability with time, before and after saturation, at different gas injection pressures (intact sample 3L).	46
Fig. 5.19	Gas permeability of the intact sample 3L before and after saturation as a function of gas injection pressure (intact sample 3L).....	47
Fig. 5.20	Removed sample 3L after the end of the test (left: healed shear plane, centre: zoomed in view, right: punched plate with shear mark).....	48
Fig. 5.21	Test for visualisation of fissures by Injection of artificial resin traced with uranine (left: central borehole with injected traced artificial resin; right: detailed view around the central borehole)	48
Fig. 5.22	Visualisation of fissures by scanning (only fissures crossing the central borehole).....	49

Fig. 6.1	FE model (2D) used for numerical simulation on water and gas injection test at BET test gallery.....	57
Fig. 6.2	Detailed view of the selected FE model (2D) used for basic numerical investigations of borehole sensor BET 2 on water and gas interaction	59
Fig. 6.3	Water pressure and gas pressure values – experimental findings vs. calculation results.....	60
Fig. 6.4	Calculated radial displacements at borehole contour zone and in the surrounding rock mass as a result of basic hydro-mechanical coupled numerical simulation of the BET 2 water and gas injection tests.....	61
Fig. 6.5	Calculated water saturation degree at borehole contour zone and in the surrounding rock mass as a result of basic hydro-mechanical coupled numerical simulation of the BET 2 water and gas injection test intervals	63
Fig. 6.6	Calculated water and gas pressure in comparison with saturation degree values as a result of basic hydro-mechanical coupled numerical simulation of the first BET 2 gas injection test interval	64
Fig. 6.7	Calculated water pressure at borehole contour zone with different water permeability values as a result of advanced hydro-mechanical coupled numerical simulation including the gallery excavation as well as the borehole excavation and the first water pressure testing intervals.....	66
Fig. 6.8	Calculated pore water pressure as a result of advanced hydro-mechanical coupled numerical simulation of gallery excavation.....	67

List of tables

Tab. 4.1	Sequence of in-situ testing.....	17
Tab. 5.1	Results of water permeability testing (values with an asterisk (*)) not reliable due to gas in the system.....	31
Tab. 5.2	Gas entry pressures (gas frac at BET 1 is marked with an asterisk (*))....	35
Tab. 5.3	Apparent gas permeabilities for the BET boreholes	36
Tab. 5.4	Apparent gas permeabilities for BMB 3 and BMB 4	37
Tab. 6.1	Material parameters determined for Opalinus clay and associated with the constitutive equations	56

**Gesellschaft für Anlagen-
und Reaktorsicherheit
(GRS) mbH**

Schwertnergasse 1
50667 Köln

Telefon +49 221 2068-0

Telefax +49 221 2068-888

Forschungszentrum

85748 Garching b. München

Telefon +49 89 32004-0

Telefax +49 89 32004-300

Kurfürstendamm 200

10719 Berlin

Telefon +49 30 88589-0

Telefax +49 30 88589-111

Theodor-Heuss-Straße 4

38122 Braunschweig

Telefon +49 531 8012-0

Telefax +49 531 8012-200

www.grs.de

ISBN 978-3-939355-36-6